DEPTH DETERMINATION BY WAVEFORM MODELING OF EARTHQUAKES ALONG THE OUTER RISE REGION OF THE KURIL ISLANDS

A Thesis

Presented to the

Faculty of

California State Polytechnic University, Pomona

In Partial Fulfillment

Of the Requirements for the Degree

Master of Science

In

Geological Sciences

By

Hannah P. Mejia

2014

SIGNATURE PAGE

THESIS: DEPTH DETERMINATION BY WAVEFORM MODELING OF EARTHQUAKES ALONG THE OUTER RISE REGION OF THE KURIL ISLANDS

AUTHOR: Hannah P. Mejia

DATE SUBMITTED: Summer 2014
Geological Sciences Department

Dr. Jascha Polet
Thesis Committee Chair
Geological Sciences

[redacted] 7/7/14

Dr. Jonathan Nourse
Department Chair
Geological Sciences

[redacted] 7/2/14

Dr. Stephen Osborn
Geological Sciences

[redacted]

Dr. Jeffrey Marshall
Geological Sciences

[redacted] 7/2/14

ACKNOWLEDGEMENTS

I want to thank my advisor Dr. Jascha Polet for allowing me to work on this project and giving me guidance throughout my undergraduate and continuing graduate career. I also want to thank my husband for putting up with my endless research. This project was partially supported through a National Earthquake Hazard Reduction Program (NEHRP) grant.

ABSTRACT

We present our results of waveform modeling of teleseismic P-waves for the purpose of determining improved locations of earthquakes in the outer rise area near the Kuril Islands. A series of large outer rise and interface events occurred in this area from 2006-2009. The depth and timing of these earthquakes may provide important insight into existing models of the modulation of the state of stress in the outer rise by subduction coupling and the seismic cycle. In the most simple of these models, tensional earthquakes generally occur at shallower depths in the outer rise, while compressional events occur at greater depths. After an interface earthquake, tensional events will occur in the outer rise at greater depths; whereas compressional events typically become non-existent. However, the hypocentral depths of outer rise earthquakes are poorly constrained by routine analysis. Furthermore, outer rise events also tend to produce complex waveforms due to the 3-D nature of the velocity structure near the trench. We determined improved depths for a number of Kuril Island outer rise earthquakes by comparison of 1-D synthetics with teleseismic P-wave data. By examining the spatio-temporal patterns of outer rise and interface events, we find the most simple of outer rise stress loading models may not be appropriate to describe the Kuril subduction zone and additional mechanisms may be required, such as dynamic stress triggering and/or strong local stress heterogeneity.

TABLE OF CONTENTS

LIST OF TABLES

LIST OF FIGURES

CHAPTER ONE

INTRODUCTION

Along the Kuril island arc (Figure 1), the Pacific Plate is subducting beneath the Okhotsk microplate, part of the larger North American Plate, at a rate of approximately 8 cm per year.

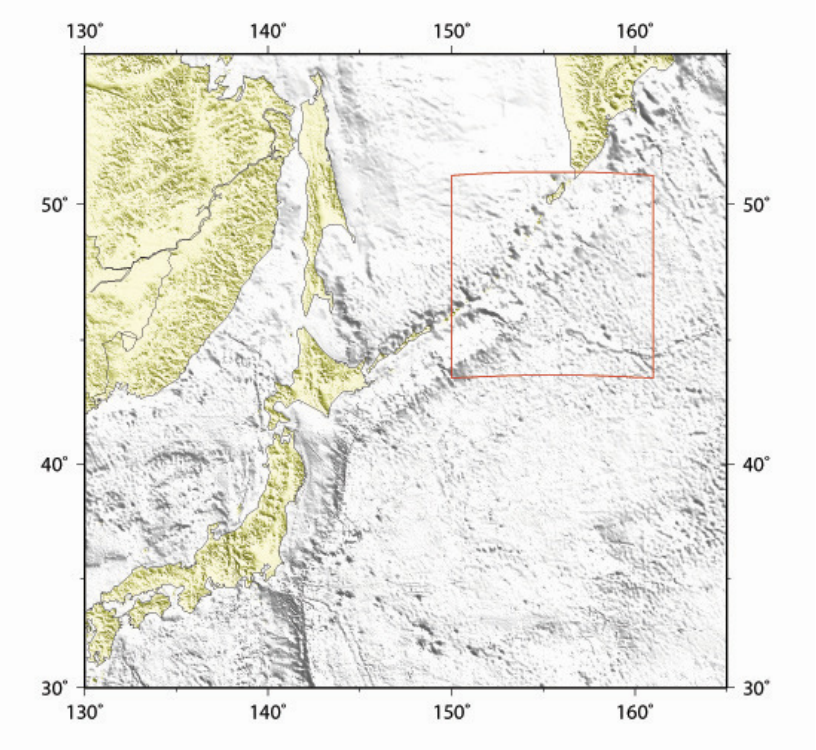

Figure 1. Overview map showing location of the Kuril Island chain. Red box shows inset location of more detailed map in Figure 12.

As a response, the Kuril subduction zone has experienced large interface earthquakes. Historically, there have been large tsunami producing events discovered through

historical document investigation and paleotsunami studies (Satake, 1983; Pacheco et al., 1993; Nanayama et al., 2003). Unusually large tsunami-generating earthquakes occur, on average, once every 500 years (Nanayama et al., 2003).

Large interface earthquakes occur along a locked portion of a subduction zone between the overriding and subducting plates (Figure 2). The coupled region along the interface is limited by the updip and downdip depths of the seismogenic zone. Understanding the area bounded by the updip and downdip extent of seismic coupling provides insight into the maximum magnitude earthquake potential of a subduction zone.

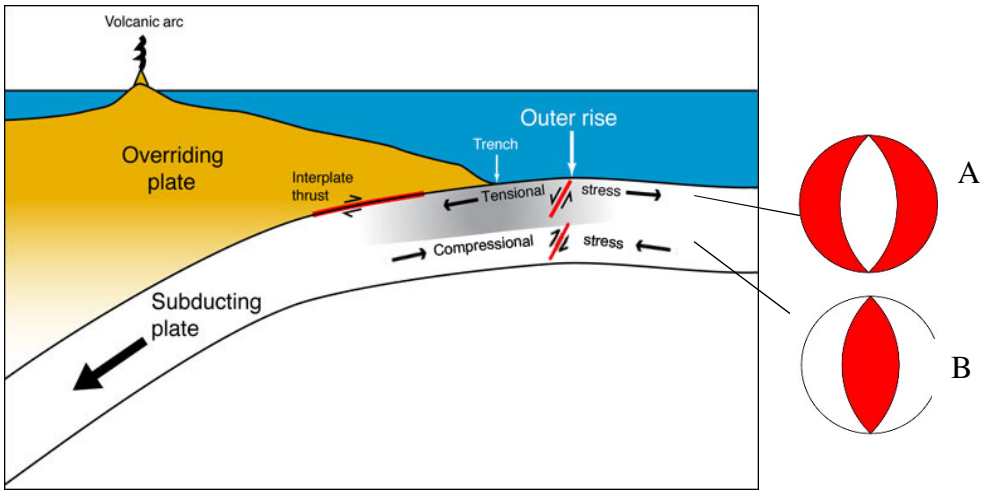

Figure 2. Diagram showing the location of the outer rise region of a subducting plate. Tensional and compressional stresses occur in the outer rise region. (A) Example of tensional focal mechanism. (B) Example of compressional focal mechanism. Both focal mechanism are created assuming a N-S striking, 45° dipping fault plane. Adapted from Geist et al. (2009).

The updip limit is controlled both by the amount of sedimentation along the trench and a critical temperature of approximately 150°C (Moore & Schaffer, 2001; Schwartz & DeShon, 2007). Large interface earthquakes and subsequent aftershock locations are used to establish the downdip limit of seismic locking to aseismic slip (Tichelaar & Ruff, 1993). The downdip limit of the seismogenic portion of a subduction zone is also controlled by temperature. Slip generally occurs at temperatures lower than 350°C (Hyndman et al., 1997). For the Kuril subduction zone, the seismically locked portion extends down to 37 and 43km downdip of the trench axis (Tichelaar & Ruff, 1993).

In the last few decades, there have been numerous subduction events above magnitude 7, including several above magnitude 8, in the Kuril region (Table 1).

Table 1

Large Interface Events since 1990
With Accompanying Magnitudes
Determined from GCMT Catalog
(Ekström et al., 2012; Dziewonski et al., 1981)

Date	Moment Magnitude (Mw)
12/22/1991	7.5
10/4/1994	8.2
10/9/1994	7.1
12/3/1995	7.9
2/7/1996	7.1
11/15/2006	8.3

Numerous events above a magnitude 8 have occurred along this region since 1923. The largest event in this area was a magnitude 9 in 1952 along the northern segment of the Kuril trench (Figure 3). Most recent event, a M8.3, occurred in 2006. In 1994, a M8.3 occurred along the southern portion of the Kuril Arc. A M8.6 occurred in 1963. A M8.4 occurred in 1958. The largest event, a M9, occurred in 1952.

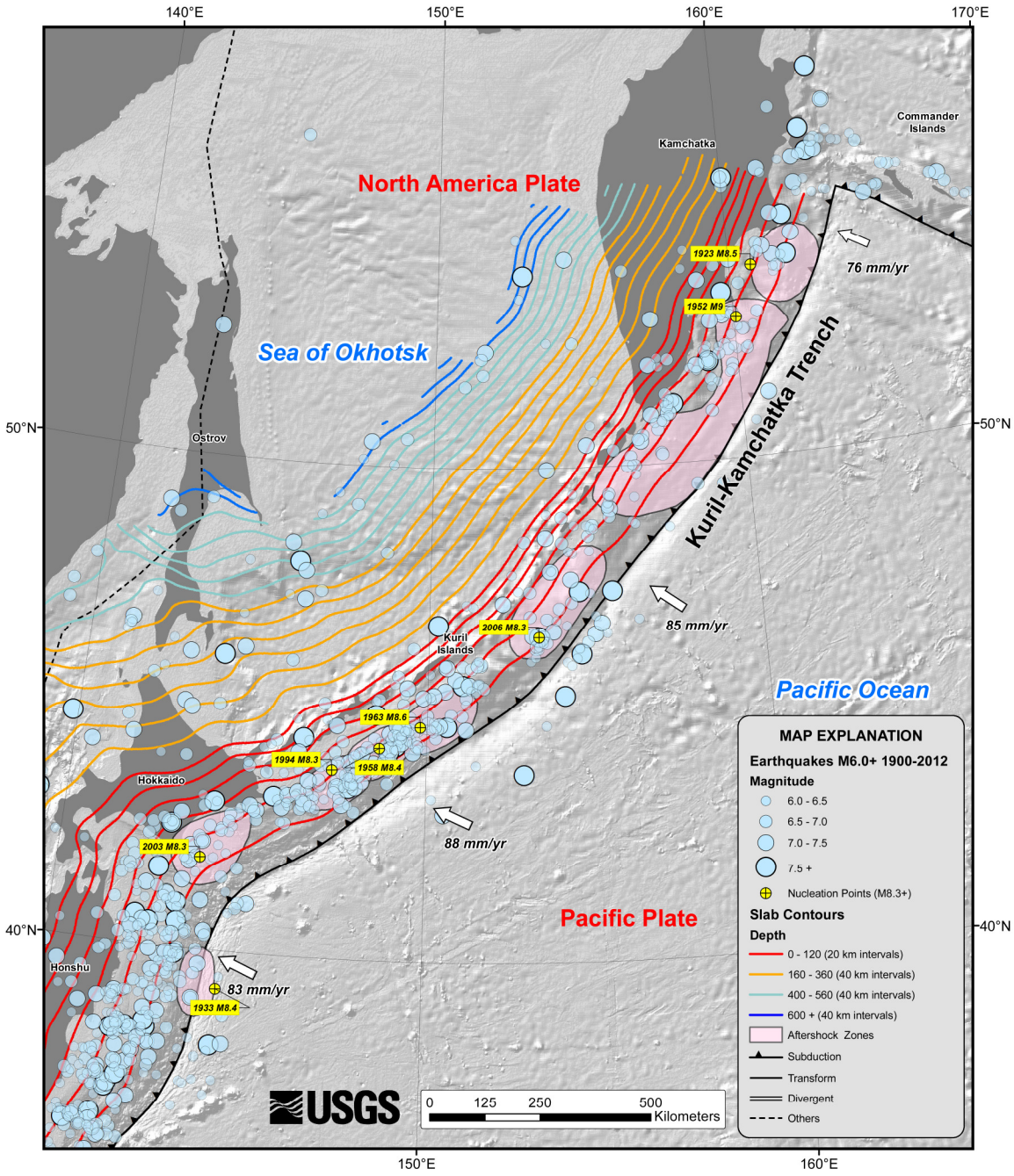

Figure 3. Historical seismicity map for the Kuril region. Pink areas represent the interface rupture area. Taken from "Tectonic Summary: Seismotectonics of the Kuril-Kamchatka Arc" (n.d.).

The most recent large interface event occurred in 2006, with a magnitude of 8.3. Interface events are often associated with intraplate events, earthquakes that do not occur on the boundary between subducting and overriding plates, but within (most commonly) the subducting plate. The outer rise is a region oceanward of the subducting trench. A topographic high is present before the trench caused by the flexure of the plate before subduction. The bending of the plate before subduction creates shallow tensional stresses and deeper compressional stresses (Figure 2). The temporal and spatial relationships of earthquakes in the outer rise intraplate region can shed light on the nature of coupling of the plate boundary (Christensen & Ruff, 1983 & 1988; Lay et al., 1989; Liu & McNally, 1993; Ammon et al., 2008; Lay et al., 2009; Obana et al., 2012). On average, twenty outer rise earthquakes between magnitudes 5 and 7 occur per year worldwide (Liu & McNally, 1993). A few months after the 2006 Kuril interface earthquake, an Mw 8.1 extensional earthquake occurred in the outer rise (Ammon et al., 2008; Lay et al., 2009). As shown by various authors (Christensen & Ruff, 1983 & 1988; Lay et al., 1989; Liu & McNally, 1993; Igarashi et al., 2003; Ammon et al., 2008; Lay et al., 2009; Obana et al., 2012), the coupling, or locking, of a subduction zone may be assessed by examining the depth, timing relative to an interface event, and tensional or compressional nature of the intraplate events assuming a model of the relationship of the stress in the outer rise with interface loading.

Compressional events are typical in coupled zones prior to a large interface event and tensional events primarily occur after a large interface event (Christensen & Ruff, 1983 & 1988; Lay et al., 1989; Liu & McNally, 1993; Igarashi et al., 2003; Ammon et al., 2008; Lay et al., 2009; Figure 4). The lithosphere is considered to be a thin elastic plate

that is influenced by a downward flexure at the subduction trench, causing tensional stresses at the upper most portion of the lithosphere and compressional stresses along the bottom portion (Christensen & Ruff, 1983). In contrast, with uncoupled subduction zones, tensional events can occur at any time due to the gradual release of seismic energy (Christensen and Ruff, 1983).

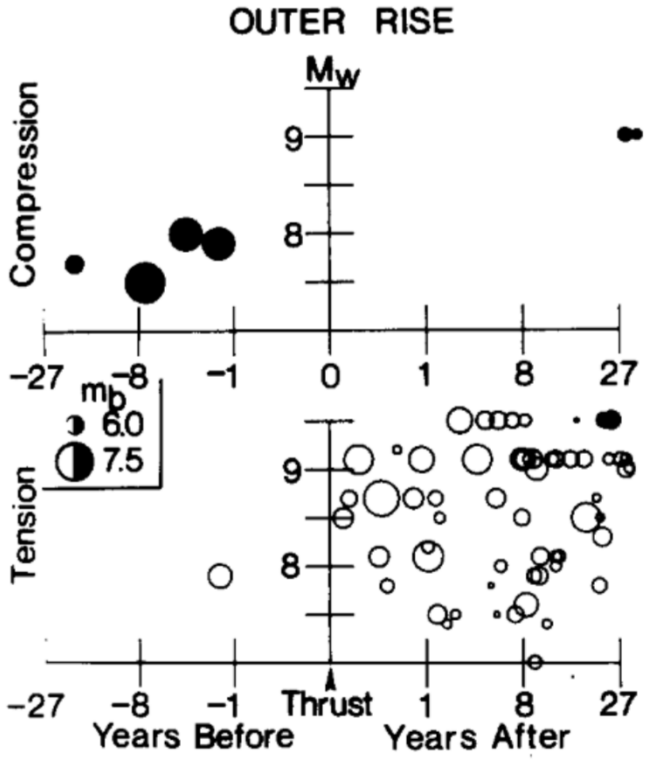

Figure 4. Outer rise events occurring pre and post interface event. Compressional events occur mainly before an interface event and tensional events occur after. Plotted relative to magnitude and time of the interface event. Taken from Lay et al. (1989).

Before the 2011 Tohoku earthquake, tensional events occurred shallower than 20 km deep and compressional events occurred at about 40 km deep in the outer rise updip

from the area that ruptured. After the earthquake, tensional events occurred down to 40 km (Obana et al., 2012). This phenomenon can be explained by plate bending and a redistribution of plate stresses. The outer rise compressional events exhibited by coupled subduction zones, therefore, may have potential to be used as a precursory signal for large interface events (Christensen and Ruff, 1988).

A majority of outer rise faults in the Kuril Islands region have a strike parallel to the trench. Analysis of intermediate depth (100-200km) intraplate events and events downdip of the trench reveal a similar fault plane pattern (Astiz et al., 1988). Subducted outer rise faults may be responsible for intermediate depth and deep earthquakes (Astiz et al., 1988). The compressional and tensional nature of intermediate depth earthquakes located downdip from the trench are potentially an indicator of coupling along the interface (Jiao et al., 2000). Differing from outer rise events, intermediate depth compressional events occur after a large interface event and tensional earthquakes occur prior to a large subduction event (Lay et al., 1989).

Age and thickness of the subducting plate may also influence the depth of compressional and tensional events in the outer rise. Thicker older lithosphere allows compressional events to occur deeper. Tensional events tend to occur above the 450° C isotherm (Jackson et al., 2008). The Pacific plate in the region of the Kuril Islands is older than 100 Ma (Lay et al., 2009) and, therefore, the lithosphere has a thickness between 70 and 100km (Hanks, 1971). In many areas, the 450 degree isotherm appears to represent a transition from the shallower outer rise tensional events to deeper compressional events (Seno & Yamanaka, 1996). Earthquake activity ceases around 600° C (Jackson et al., 2008).

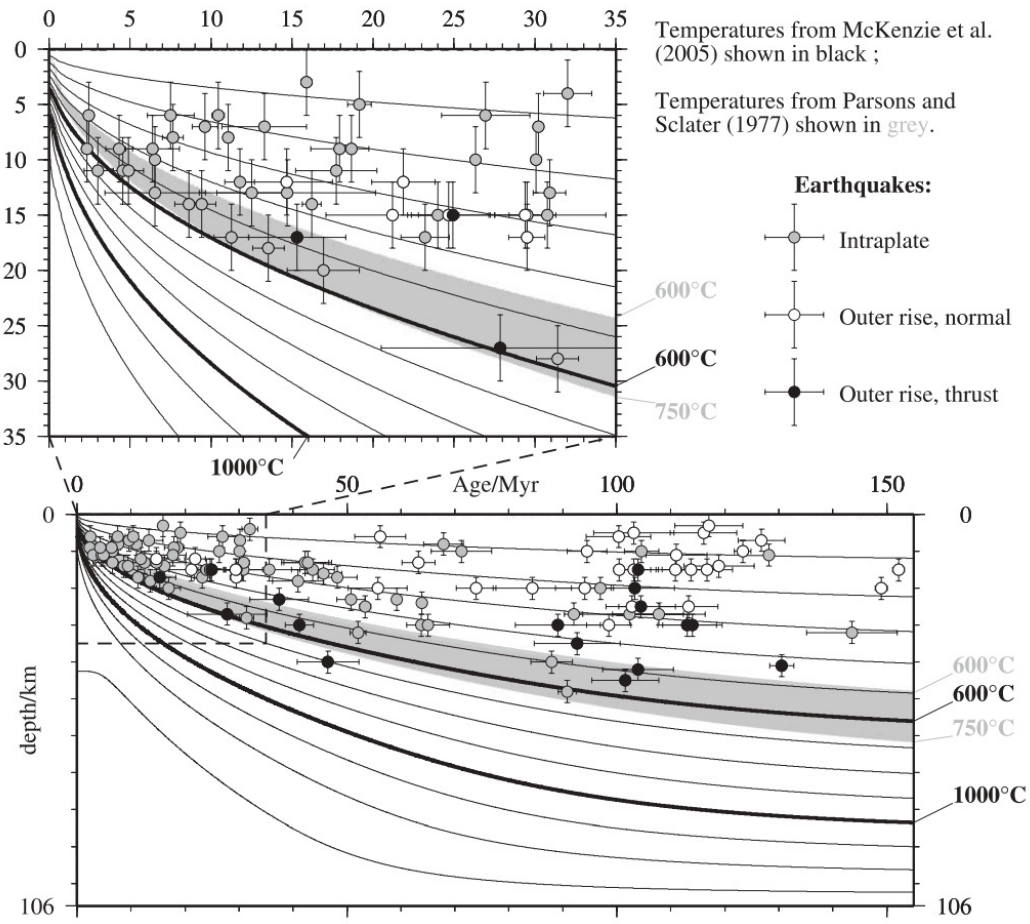

Figure 5. Age of lithosphere plotted with depth and temperature. Gray circles represent intraplate events, open circles represent tensional outer rise events, and black circles represent compressional outer rise events. Lines represent temperature isotherms. Taken from Jackson et al. (2008).

The balance of forces in the outer rise can cause depth changes to the neutral stress surface between compressional and tensional events. Prior to a large interface event, the forces along a locked subduction zone cause a compressive tangential force allowing for compressional events to occur shallower in the outer rise. Conversely, in an un-coupled subduction zone, a tensile load along the trench causes deeper compressional events. According to Liu & McNally (1993), the Kuril subducting trench is locked

allowing for a compressive tangential force and shallower compressional outer rise events prior to a large interface event (Figure 6).

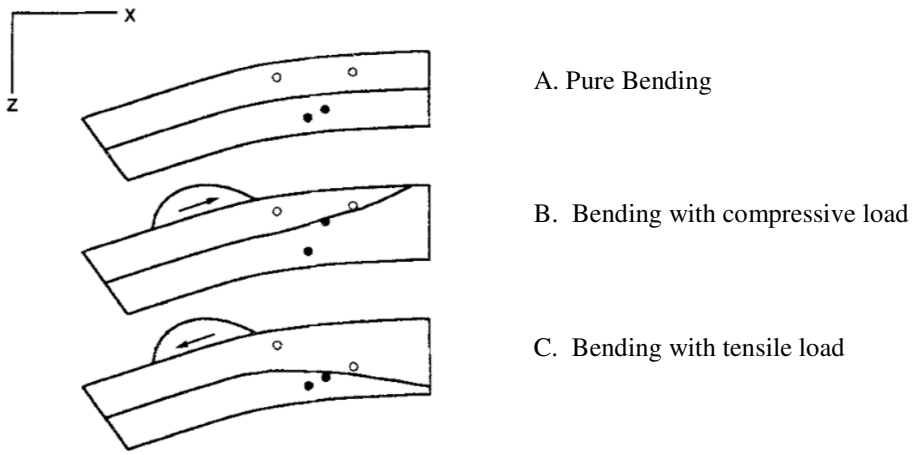

Figure 6. Outer rise force scenarios. (A) Pure bending with no additional plate loading. (B) Bending with compressive load causing shallower compressional earthquakes in the outer rise. (C) Bending with tensile load causing deeper compressional earthquakes in the outer rise. Open circle are tensional events. Filled circles are compressional events. Modified from Liu & McNally (2003).

Hypocentral depths of earthquakes that occur in outer rise regions of subduction zones are difficult to constrain. The depths provided in the global centroid moment tensor (GCMT) catalog are commonly between 10-15 kilometers, which may not indicate the true depth of the event, especially since these depths are often held fixed in the GCMT inversion. A shallow depth is fixed in the inversion due to instabilities in the inversion (Konstantinou & Rontogianni, 2011; Ekström et al., 2012). Depths of outer rise events are also not well constrained by using land-based seismograph networks (Obana et al.

2012). It is, however, important to determine accurate depths, because, as discussed previously, the earthquakes that occur in the outer rise could provide information about the seismic cycle of a subduction zone. In an un-coupled subduction zone, tensional events can occur at any time during the seismic cycle (Christensen & Ruff, 1983).

The Kuril outer rise region has experienced outer rise compressional events indicating a potential coupled subduction zone (Christensen and Ruff, 1983). A M5.3 outer rise compressional event occurred at 47km depth in 1990 prior to a M7.5 subduction event in 1991. The interface event was followed by a M5.6 tensional outer rise event at 17km depth in 1994. The occurrences of the compressional event prior to the large interface event, and the tensional events post thrust event indicate a locked subduction zone.

Large earthquakes have recently occurred in the Kuril Islands region, both along the interface and the outer rise. Therefore, the region provides a natural laboratory to test existing models of the effects of stress changes during the seismic cycles on outer rise seismicity and gain understanding of its spatial and temporal variations. To this end we determine more accurate depths for these events using waveform modeling. We compare synthetics seismograms computed for a range of depths to recorded waveform data for teleseismic P-waves.

CHAPTER TWO

METHODS

Focal mechanisms are used to study fault orientation and type of faulting of an earthquake. They may be created using the first motions of P-waves observed at seismic stations with varying distances and azimuths from the earthquake. Depending on the type of faulting and the location of the station relative to the earthquake, the first motion of the P-wave recorded at that station will show an up or down motion. The first motions, therefore, provide information on the type of fault motion and the fault orientation of the earthquake. First motions describe four quadrants, two compressional and two dilatational of the imaginary focal sphere surrounding the earthquake (Figure 7). If the first motion recorded on the seismogram is up, it is plotted as compressional on a lower hemispheric projection by distance and azimuth. If the first motion recorded is down, it is plotted as dilatational. The four quadrants are divided by two nodal planes; one the fault plane and the second the auxiliary plane perpendicular to the fault plane (Figure 7). Unless other factors are known, first motions alone cannot resolve the fault plane from the auxiliary plane. Combining the first motions from multiple locations can provide a complete view of the focal mechanism. Compressional, or thrust, faulting is shown on a focal mechanism with one compressional section surrounded by two dilatational sections. Conversely, tensional, or normal, faulting is shown with one dilatational section surrounded by two compressional sections (Figure 8; Stein and Wysession, 2003). Since our interest for this thesis project is in intraplate seismicity, we selected the events for our analysis by picking events with focal mechanisms that did not correspond to faulting on the subducting interface.

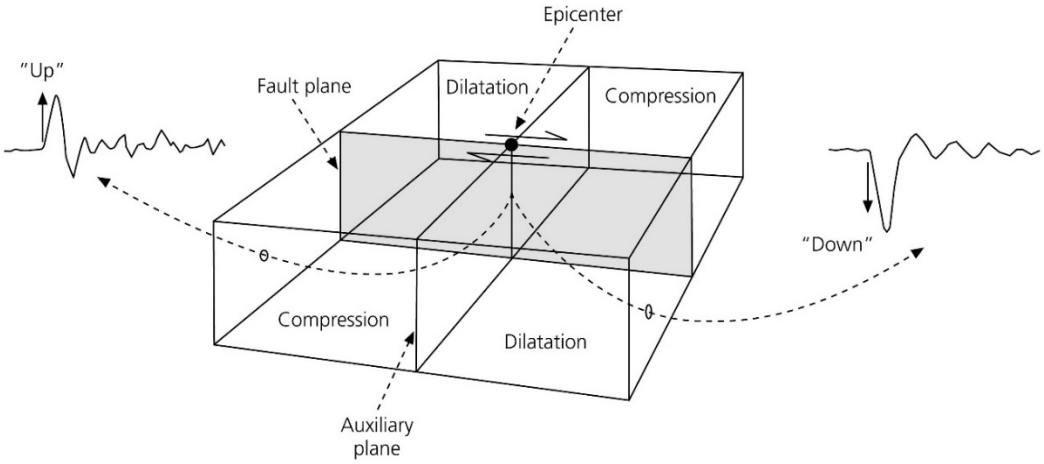

Figure 7. P-wave first motions indicative of compressional and dilatational quadrants located around a right lateral strike slip fault plane. Taken from Stein and Wysession (2003).

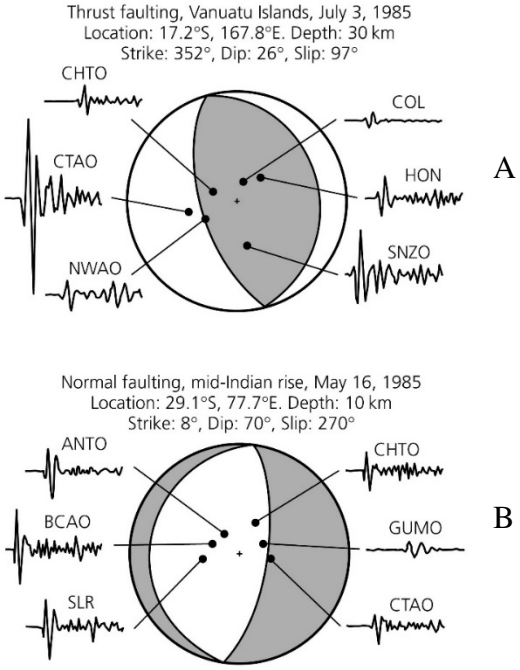

Figure 8. (A) Thrust focal mechanism with seismograms showing P-wave motions. (B) Normal faulting focal mechanism with first motions. Taken from Stein and Wysession (2003).

Similarly, focal mechanisms provide information on what type of P-wave first motions will be produced. The initial P-wave released carries a certain polarity, either up or down corresponding to a compressional or tensional quadrant respectively, that is recorded on the seismogram. However, the total P-waveforms recorded on a seismograph consists of the initial P wave and subsequent waves interacting with subsurface layers, called depth phases. These other phases produced by the earthquake also carry a polarity depending on the quadrant of the focal mechanism. The polarity of the wave will reverse when it interacts with the free surface (Stein & Wysession, 2003; Figure 9).

Waveform data was downloaded via the Incorporated Research Institutions in Seismology (IRIS) Wilber 3 interface. The data was uncompressed using the rdseed software. P-wave markers were added using TauP Toolkit (Crotwell et al., 1999). The waveforms were subsequently processed to filter out background noise and integrated to show ground displacement into displacement after removal of the instrument response. After processing, the data can be directly compared to the synthetic seismograms that we produced using different methodologies.

To calculate synthetic seismograms, seismic waves can be simulated by solving the elastic wave equation in a medium (i.e. the Earth) numerically. This wave equation is a partial differential equation that describes the elastic response in a medium to a force (or set of forces) that act inside that medium (i.e. the earthquake source). For the propagation throughout the bulk of the Earth we can model the seismic waves using simple ray corrections, which account for geometrical spreading and attenuation.

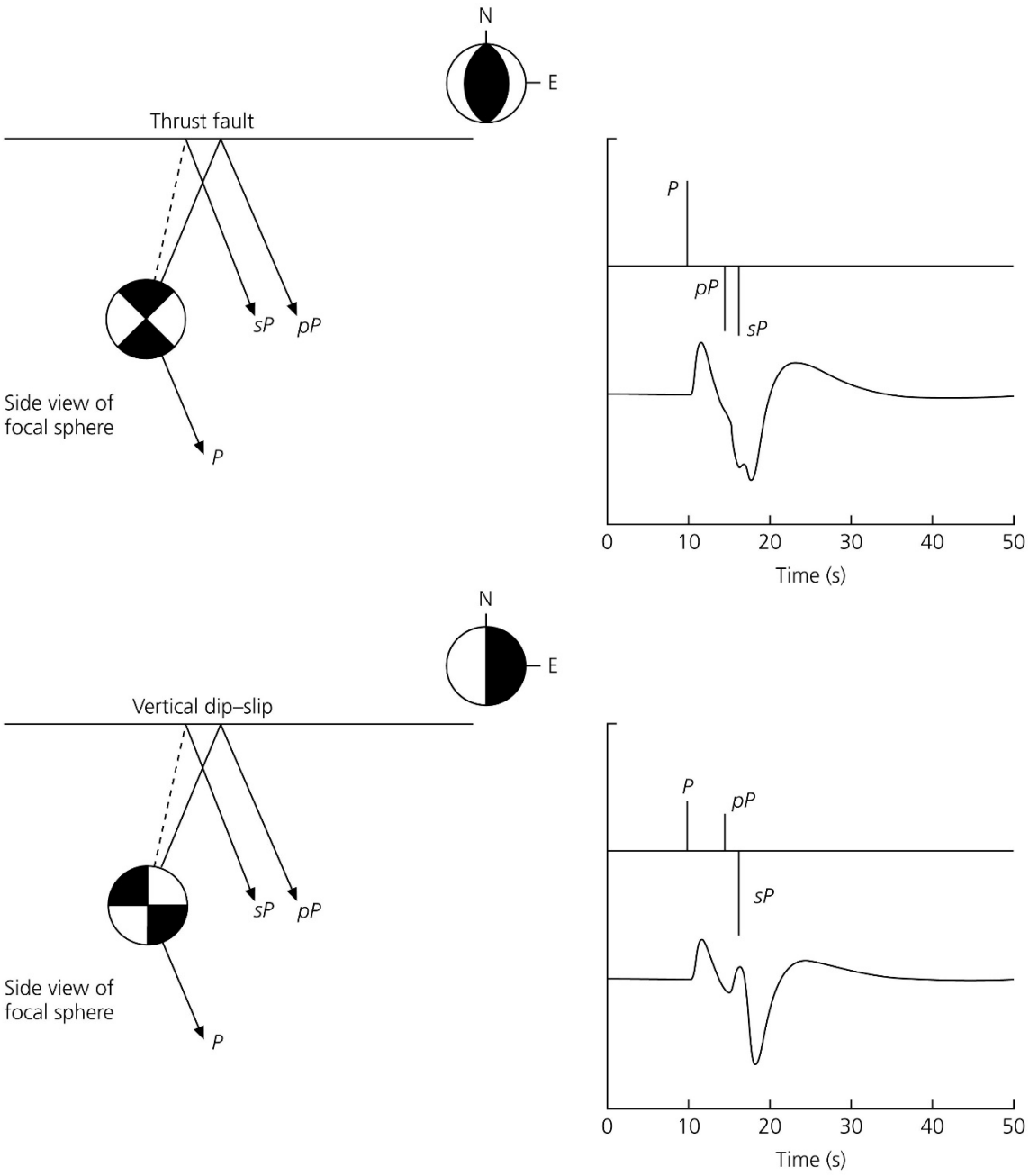

Figure 9. Focal mechanisms, in map and side view, showing initial P-wave with corresponding depth phases. Note the different polarities of the direct P-wave and depth phases for the different mechanisms and wave types. Taken from Stein and Wysession (2003).

For the near source subduction region, where the structure is far more complex, we have used two different methods to model these waves:

- Propagator Matrix Approach
- 3-D Finitie Difference Approach

The propagator matrix approach assumes an Earth model where the elastic properties (and thus the seismic velocities) only vary with depth, so that the Earth structure (at least locally) is represented by a stack of horizontal layers with different velocities and density. In this case, which is referred to as 1-dimensional, or 1-D, the response of every layer within that stack can be represented by a simple matrix, called propagator matrix, and the response of the entire stack of layers is then a multiplication of the different matrices. This method is numerically very accurate and very fast, allowing us to compute synthetic waveforms within a second.

In the 3-D finite difference method, the Earth's structure (and even topography) can vary arbitrarily in all three spatial directions. In this method, rather than modeling the elastic response of entire layers, we model the elastic response of individual cells with typical dimensions of a few hundred meters inside the medium. Because of the more complex algorithms, necessary because the response needs to be computed in six spatial directions rather than two, and the vastly larger number of elements for which the response is computed (millions of cells instead of a few layers), the 3-D finite difference method takes up to ten hours to compute waveforms in a cube with sides of about 100 km (Pitarka, 1999).

To determine more accurate depths for the outer rise earthquakes that we selected for this study earthquakes, P-waveforms from synthetics and data are compared. To

create 1-D synthetic seismograms showing first motions, a 1-D location based slice through a 2-D velocity model is taken. The velocity model from Okamoto (1994) was digitized to easily create the 1-dimensional slices (Figure 10). The model was created for a location close in proximity to the locations of the events selected for analysis. Borehole and seismic reflection data was used to create the velocity model for the Kuril region (Okamoto, 1994).

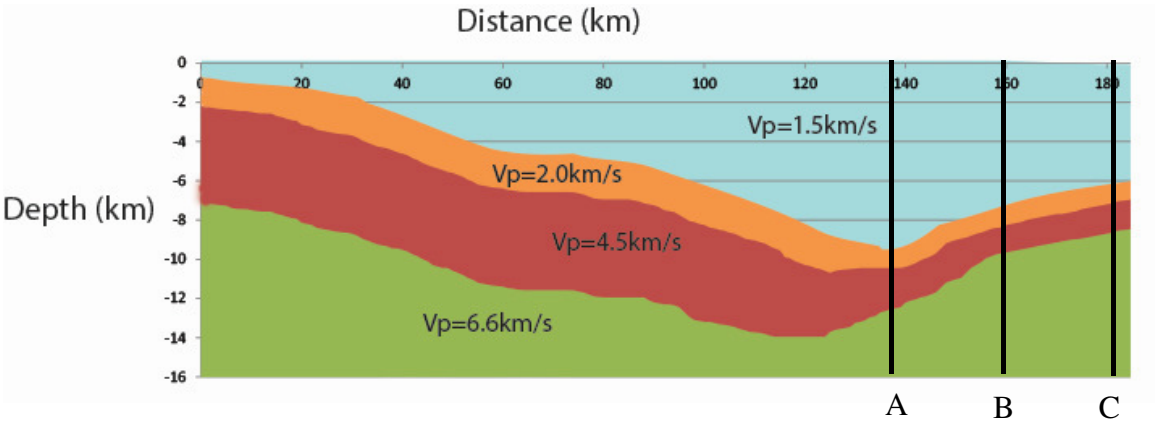

Figure 10. Digitized 2-D cross section of the Kuril Islands subduction zone P-wave velocities. Slices were taken from the (A) trench, (B) closer to the trench and (C) further to the trench. Black lines represent sections used to generate the 1-D synthetics. The orange layer with a 2km/s P-wave velocity (Vp) represents an approximately 1km thick sediment layer. The red layer with a 4.5km/s Vp represents a greater than 2km thick layer of metamorphosed sediments and volcanics. The last layer (green) with a Vp of 6.6km/s represents a metabasalt and gabbro layer that is assumed as infinitely thick (Gnibidenko et al., 1981). Digitized from Okamoto (1994).

Three sections are used depending on the location of the GCMT centroid relative to the trench. The 1-D velocity model section was used as input into a propagator matrix code to create the synthetic seismograms. The synthetics are then compared to waveform data to determine a more suitable earthquake depth (Figure 11).

Events and stations were chosen based on several criteria. Only compressional and tensional events updip and oceanward of the trench are used for analysis. Maps and cross sections generated using the GMT software (Wessel et al., 2013) and used to choose events in the outer rise by location (Figures 12 & 13). Only events after 1990 are selected due to provide optimal coverage and high quality digital data for our analysis. Events must have a magnitude between 5.1 and 6.4, ideally magnitudes 5.5 to 6.4, for clear recordings at stations with teleseismic distances greater than 30° from the event. To ensure sufficient events for analysis, we had to lower the minimum magnitude of our selection range to 5.1. Events with magnitudes lower than 5.5 only had a few acceptable stations to be used in analysis. Only the vertical component was used because teleseismic P-waveforms have an almost vertical incident angle with the surface and, therefore, will generate the largest amplitudes on the vertical component of a seismogram. Stations from all azimuths and distances between 30 and 90 degrees are used (Figure 14). Waveforms from distances shorter than 30 degrees are complex due to interference effects from rays turning within the transition zone in the upper mantle. Similarly, at distances greater than 100 degrees, diffractions from the core-mantle-boundary complicate the interpretation of teleseismic P-waveforms. Eleven events were chosen; three compressional and the remaining tensional (Table 2). Several outer rise earthquakes occurred close in time to large interface and outer rise events. Those events were excluded because too much

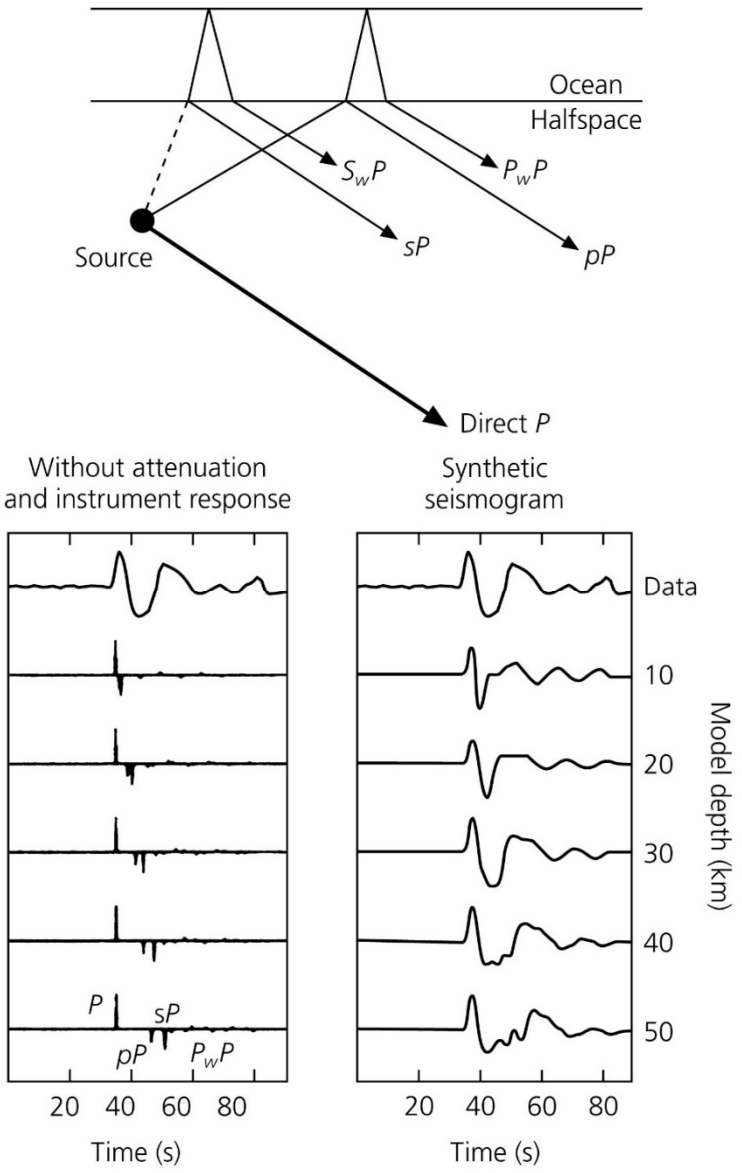

Figure 11. Data compared to synthetics for teleseismic P-waves, including depth phases, calculated for a range of depths. Synthetics most similar to data for earthquake depth of 30km. Taken from Stein and Wysession (2009).

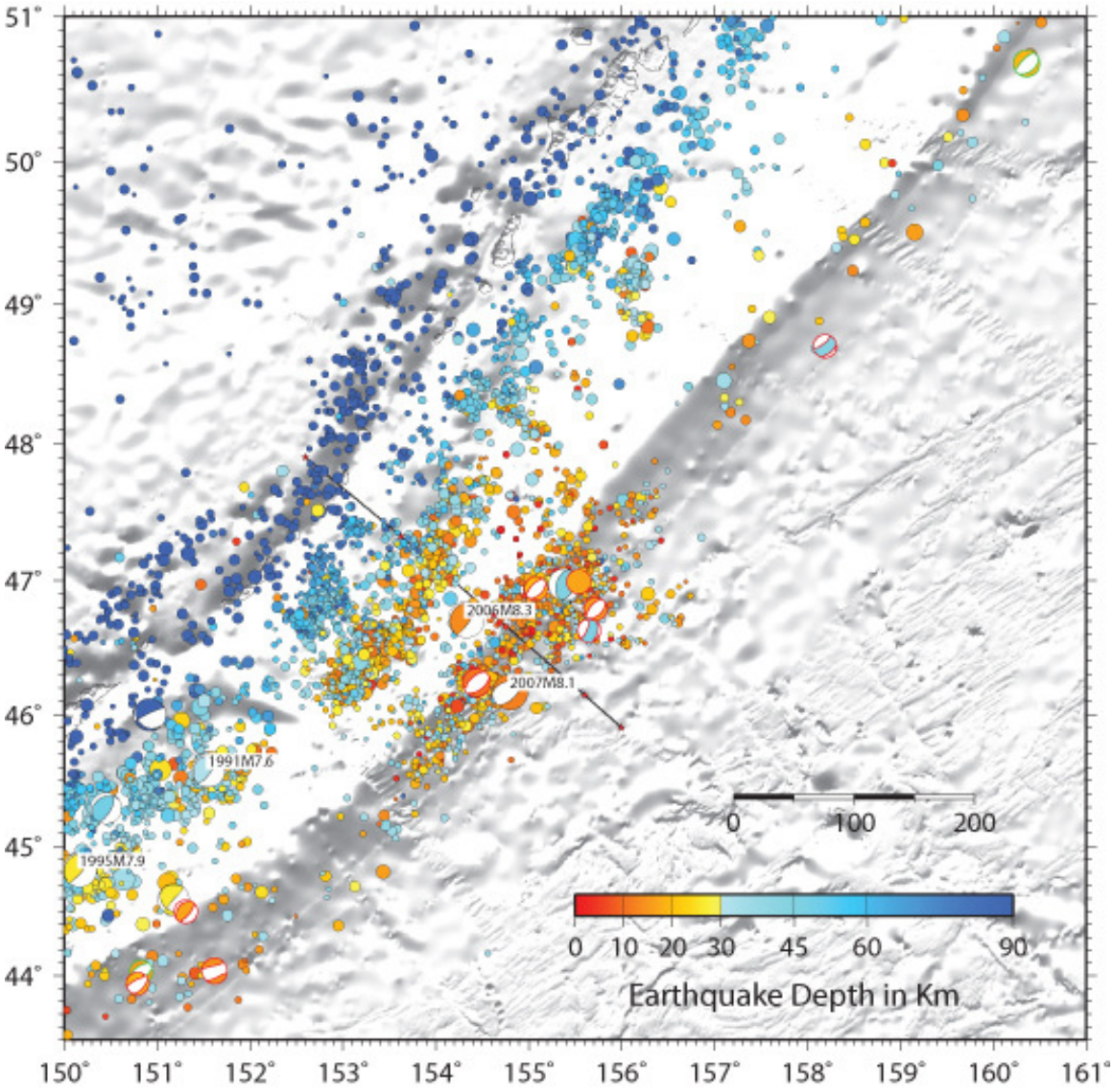

Figure 12. Map of earthquakes along the Kuril Islands. Events are scaled with size and colored by depth. Large events, both interface and outer rise, indicated by date. Focal mechanisms from GCMT catalog (Dziewonski et al., 1981; Ekström et al., 2012), circles show earthquakes from ISC catalog (Di Giacomo et al., 2014; International Seismological Centre, 2014). Colors indicate depth, symbol size scales with magnitude. Line indicates location of cross section in Figure 13.

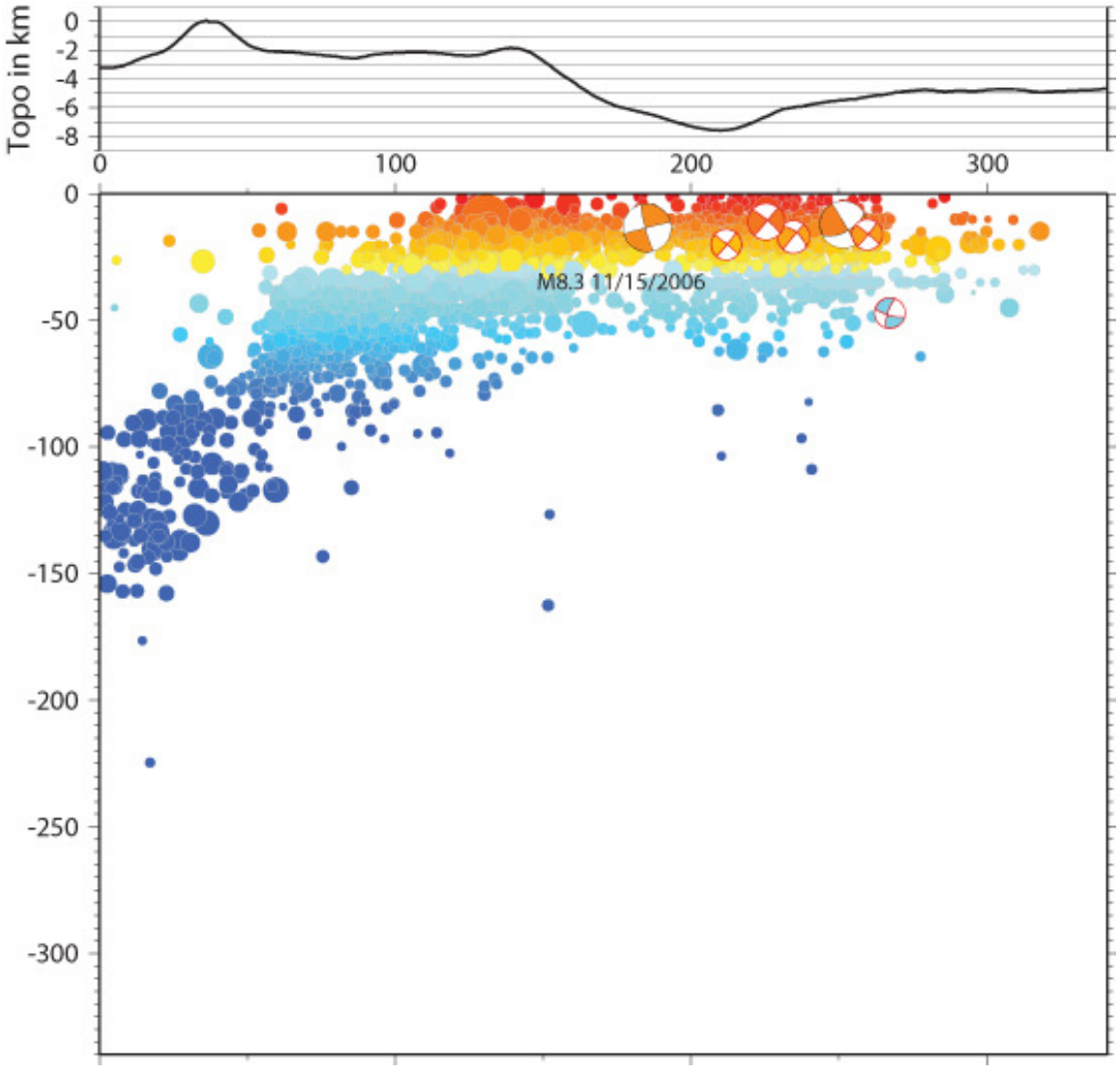

Figure 13. Cross section view of Kuril Islands region. (Top) Topographic/bathymetric profile. Trench located at the topographic low. (Bottom) Side view of focal mechanisms plotted for analyzed outer rise earthquakes. Outer rise earthquakes plotted with depth as determined from waveform analysis. Background seismicity plots as in Figure 12.

Figure 14. Azimuth map of stations used in data analysis. Map centered on the Kuril Islands.

Table 2

Events Selected for Depth Analysis Based on Synthetic Waveforms

Date	Moment Magnitude (Mw)	Hypocenter Depth (km)	GCMT Depth (km)	Mechanism
9/10/1990	5.3	23	38	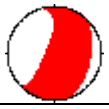
9/5/1994	5.6	33	15	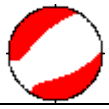
6/19/1995	5.1	33	15	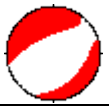
12/4/1995	5.3	42	15	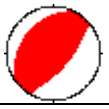
9/13/2004	5.9	8	12	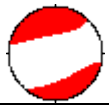
8/10/2005	5.3	31	43	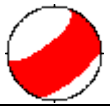
11/19/2006	5.3	12	12	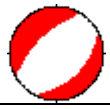
11/28/2006	5.3	10	12	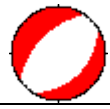
12/7/2006	6.4	16	15	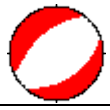
1/17/2009	5.4	22	12	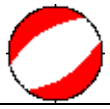
3/24/2013	6.0	8	12	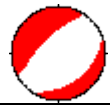

Magnitude, hypocenter and centroid depths, and mechanisms downloaded from Global Centroid Moment Tensor catalog.

residual noise washes out the smaller waves of the outer rise events. Image files were created for all events and stations to choose clear seismograms for analysis. After choosing the clear seismograms at specific stations per event, synthetics were created for a range of depths, using a propagator matrix approach after specifying strike, dip and rake parameters from the event at the specific azimuth and distance for the clear station.

CHAPTER THREE

DATA ANALYSIS

We compare recorded waveform data of teleseismic P-waves with 1D synthetic seismograms generated for a velocity model of the Kuril subduction zone by visual inspection to determine a more accurate depth than those given by the Global Centroid Moment Tensor (GCMT) catalog and other routine data processing methods. To facilitate comparison, data is plotted above synthetics, with synthetic seismograms initially calculated for a range of source depths with an interval of 5km (see the example in Figure 15). After determining which depth range of synthetics produced the best match with the data, more synthetics are created to be analyzed for every 1km change in earthquake source depth (Figure 16). Examples are shown for two events: a M5.3 tensional outer rise event which occurred on 11/28/2006 and an additional M6.0 tensional event on 3/24/2013. Comparisons with data recorded at additional stations for each of the analyzed events are provided in the appendix. The depth for the event on 11/28/2006 is determined by using three stations. Each of the stations is located between 250° and 280° in azimuth. There are very few stations located between 290° and 60° in azimuth. After analyzing two stations (Figures 15-18), a depth of 16km is determined. The depth as determined from our waveform analysis for the 11/28 event is slightly deeper than the depth given by the GCMT. For the tensional event on 3/24/2013, two stations were analyzed (Figures 19-22). The newly determined depth is 19km, which is larger than the depth provided by the GCMT. Depths determined using waveform analysis for all events analyzed are presented in Table 3. These results are also shown in the focal mechanism map of Figure 12 and cross-section of Figure 13.

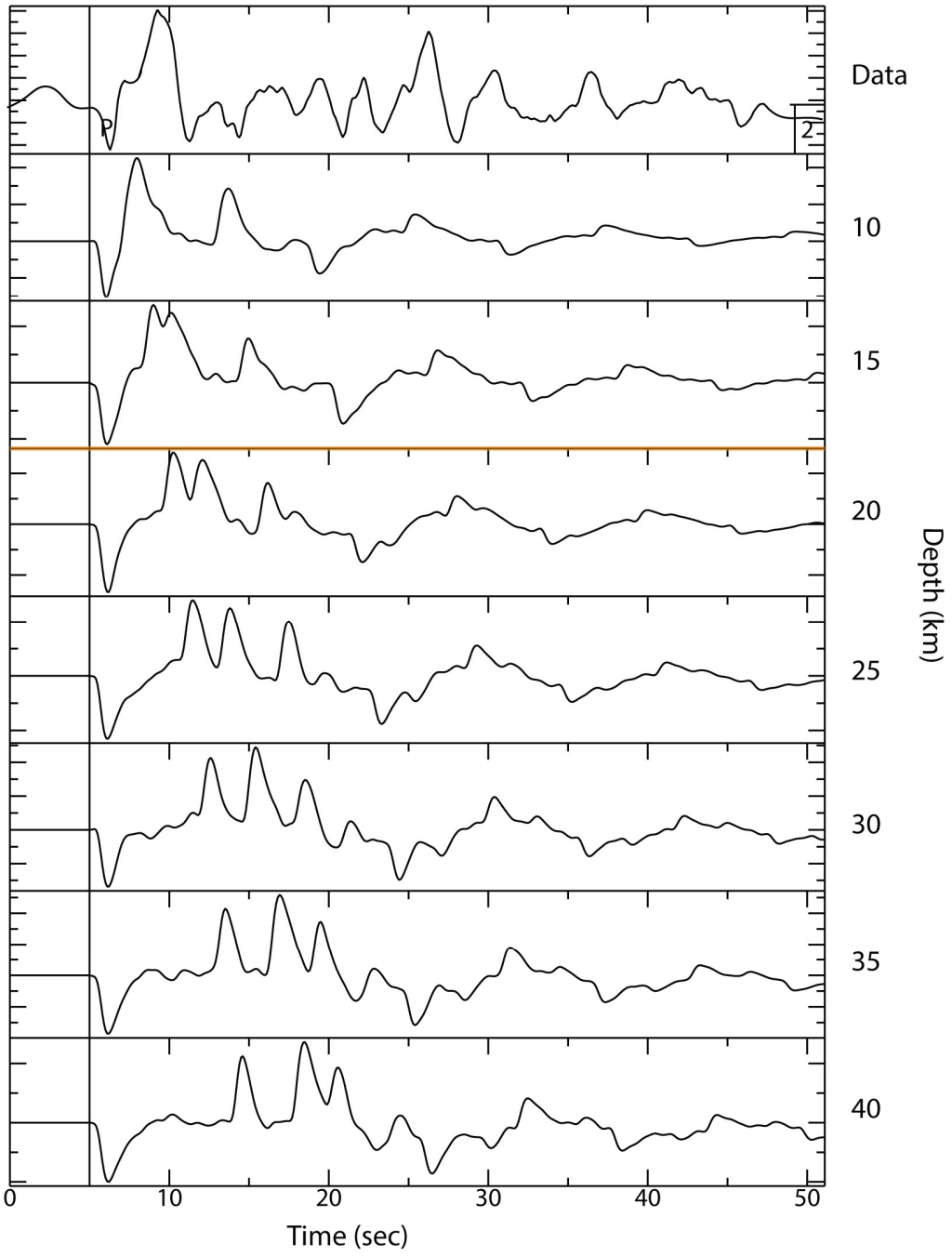

Figure 15. Synthetics for a tensional event on 11/28/2006. Station DNL located at 280° azimuth and 45° distance from event. Best match for synthetics calculated for depths between 15 and 20km (orange line).

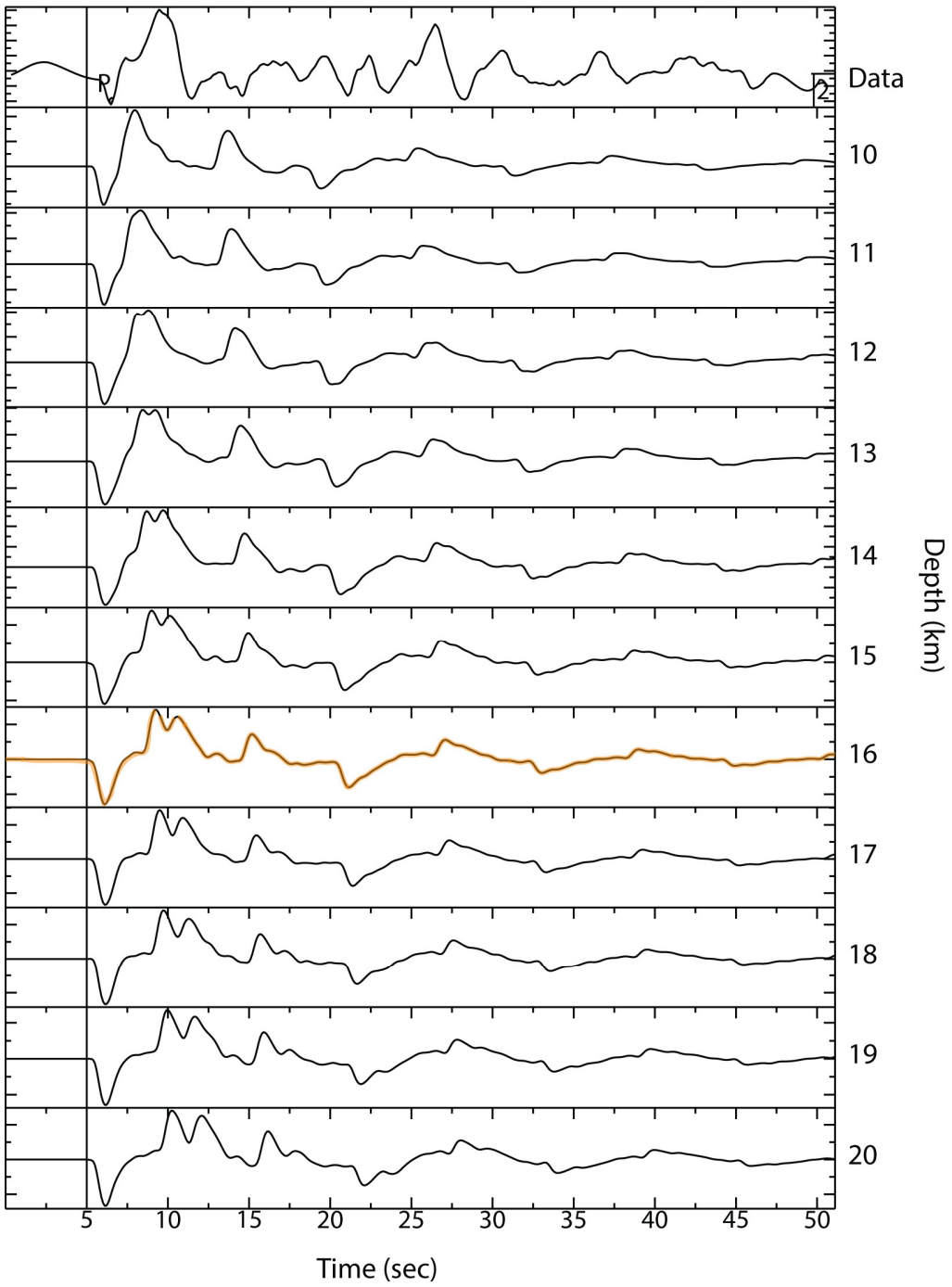

Figure 16. Synthetics for a tensional event on 11/28/2006. Station DNL located at 280° azimuth and 45° distance from the event. Best match for synthetics calculated for a depth of 16km highlighted in orange.

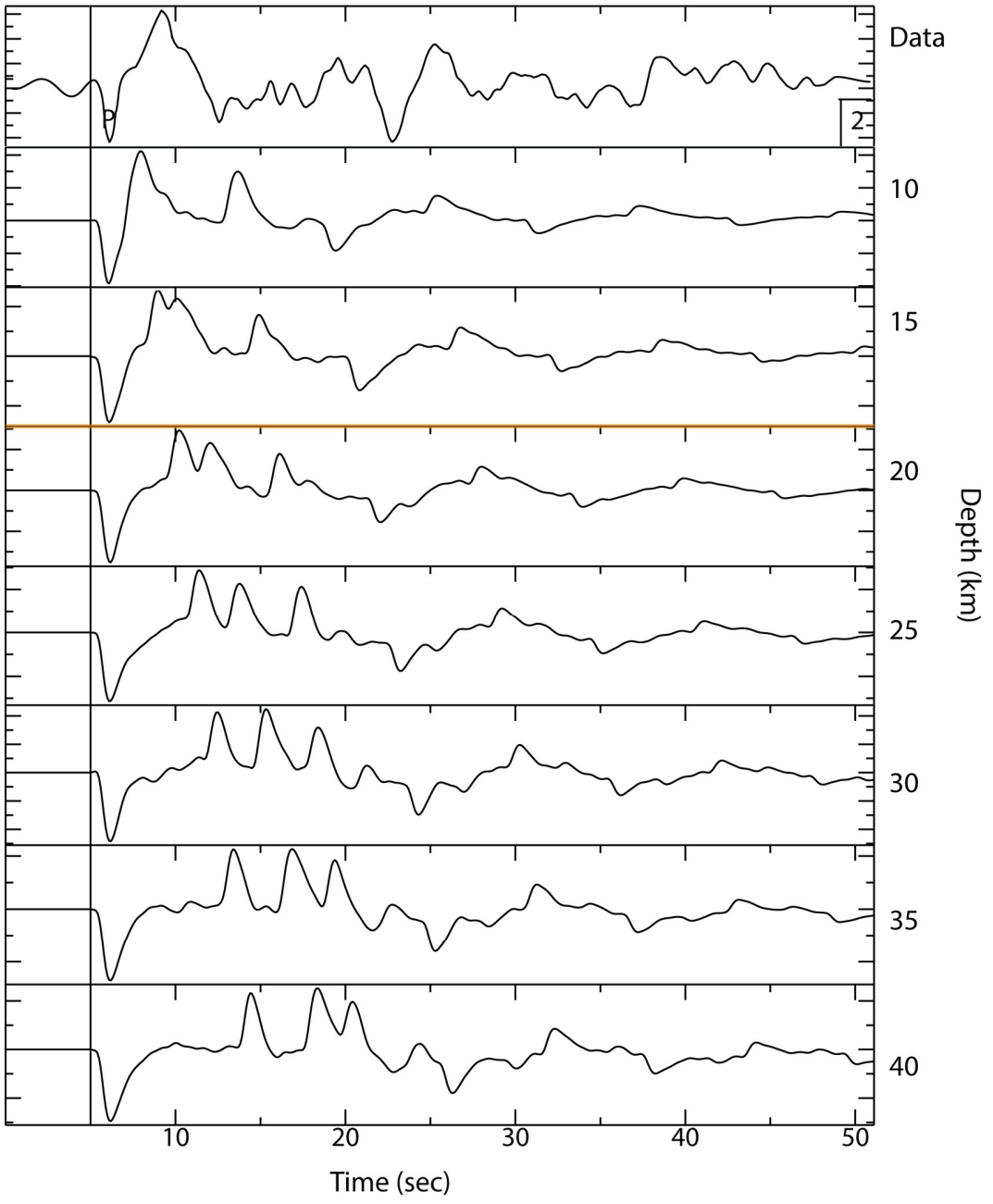

Figure 17. Sythetics for a tensional event on 11/28/2006. Station ENH located at 260° azimuth and 40° distance from the event. Best match for synthetics calculated for depths between 15 and 20km highlighted in orange.

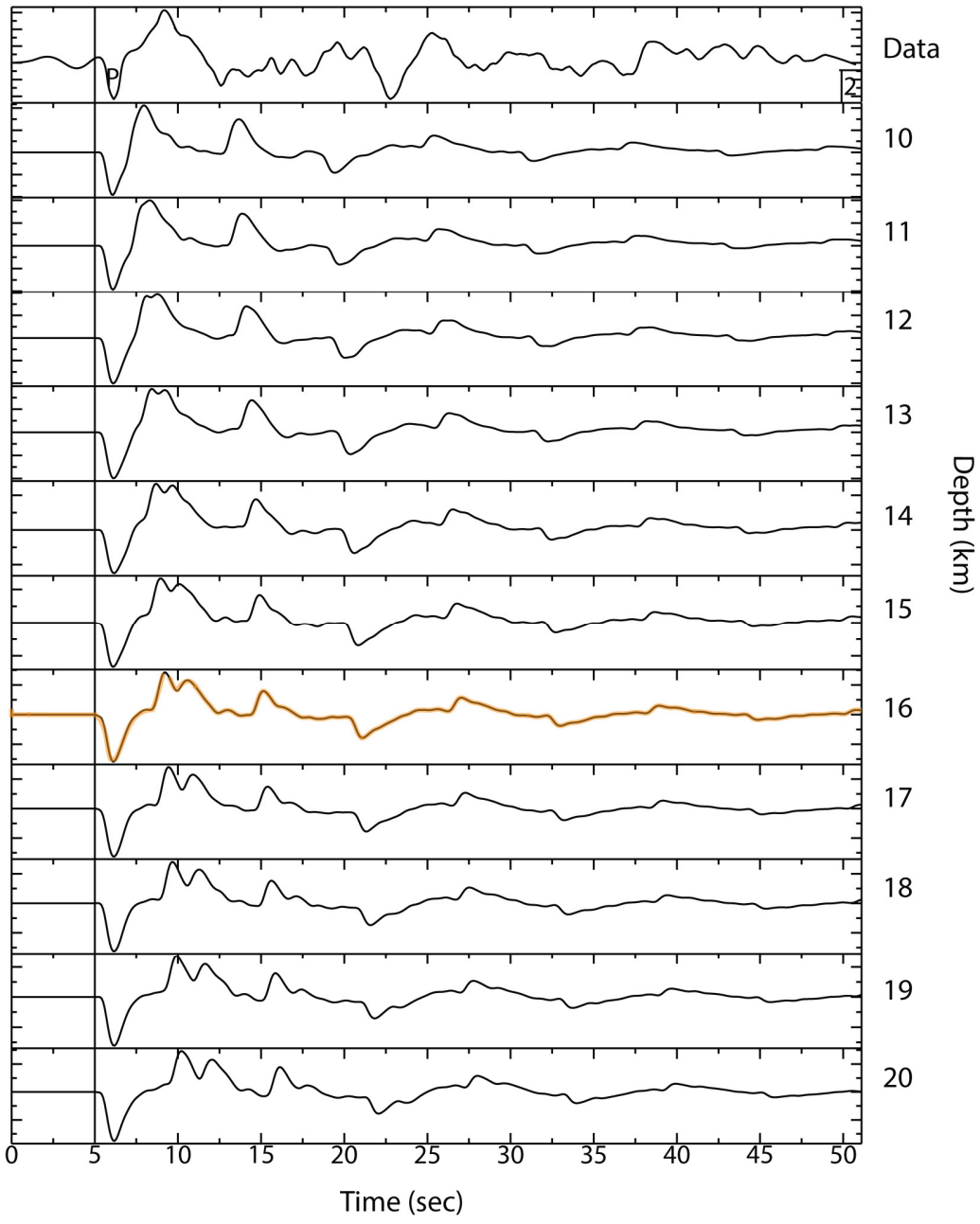

Figure 18. Synthetics for a tensional event on 11/28/2006. Station ENH occuring at 260° azimuth and 40° distance from event. Best match for synthetics calculated for a depth of 16km highlighted in orange.

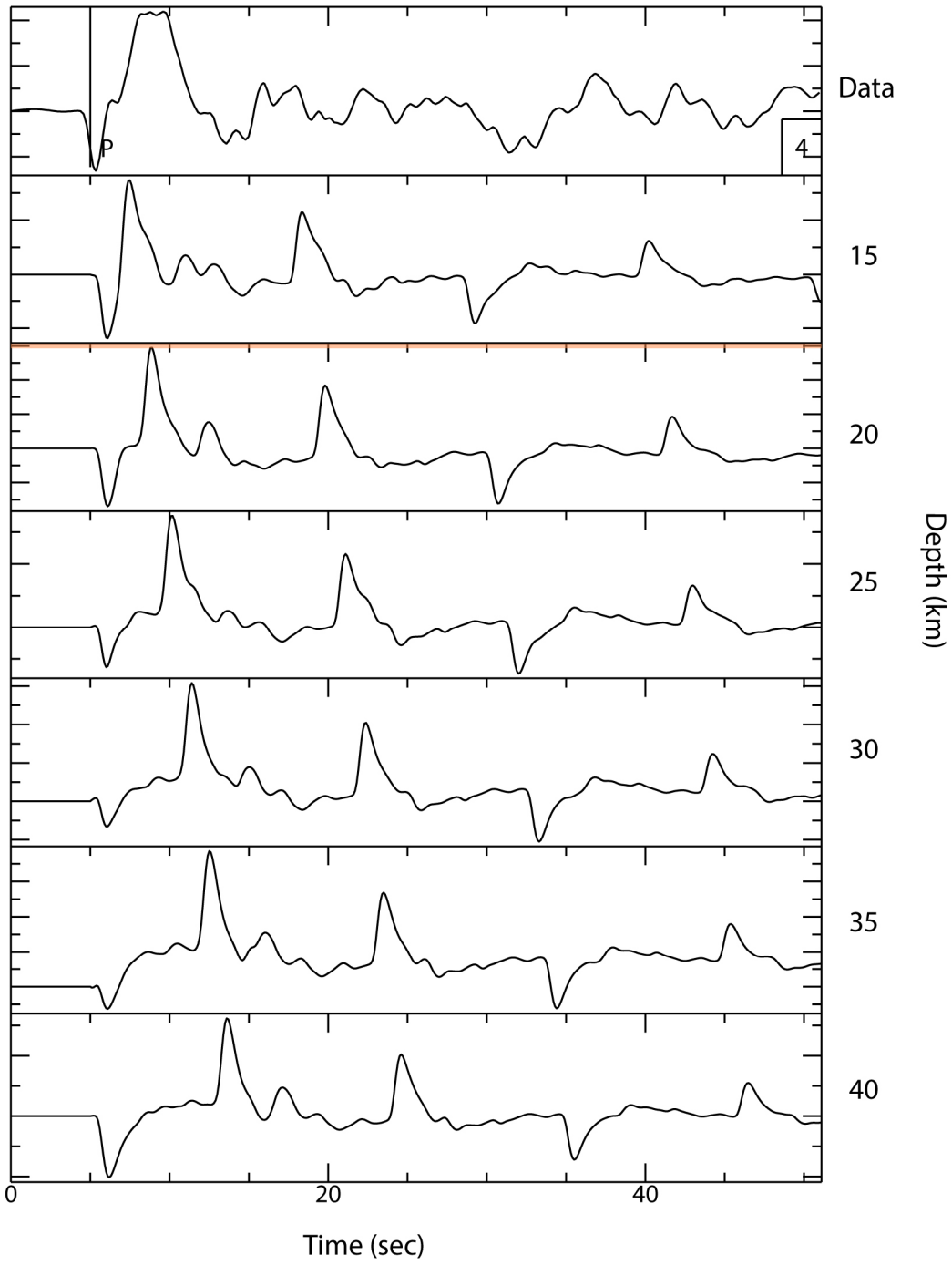

Figure 19. Synthetics for tensional event on 3/24/13. Data from station KBL located at 295° azimuth and 65° distance from earthquake. Best match for synthetics calculated for depths between 15 and 20km (orange line).

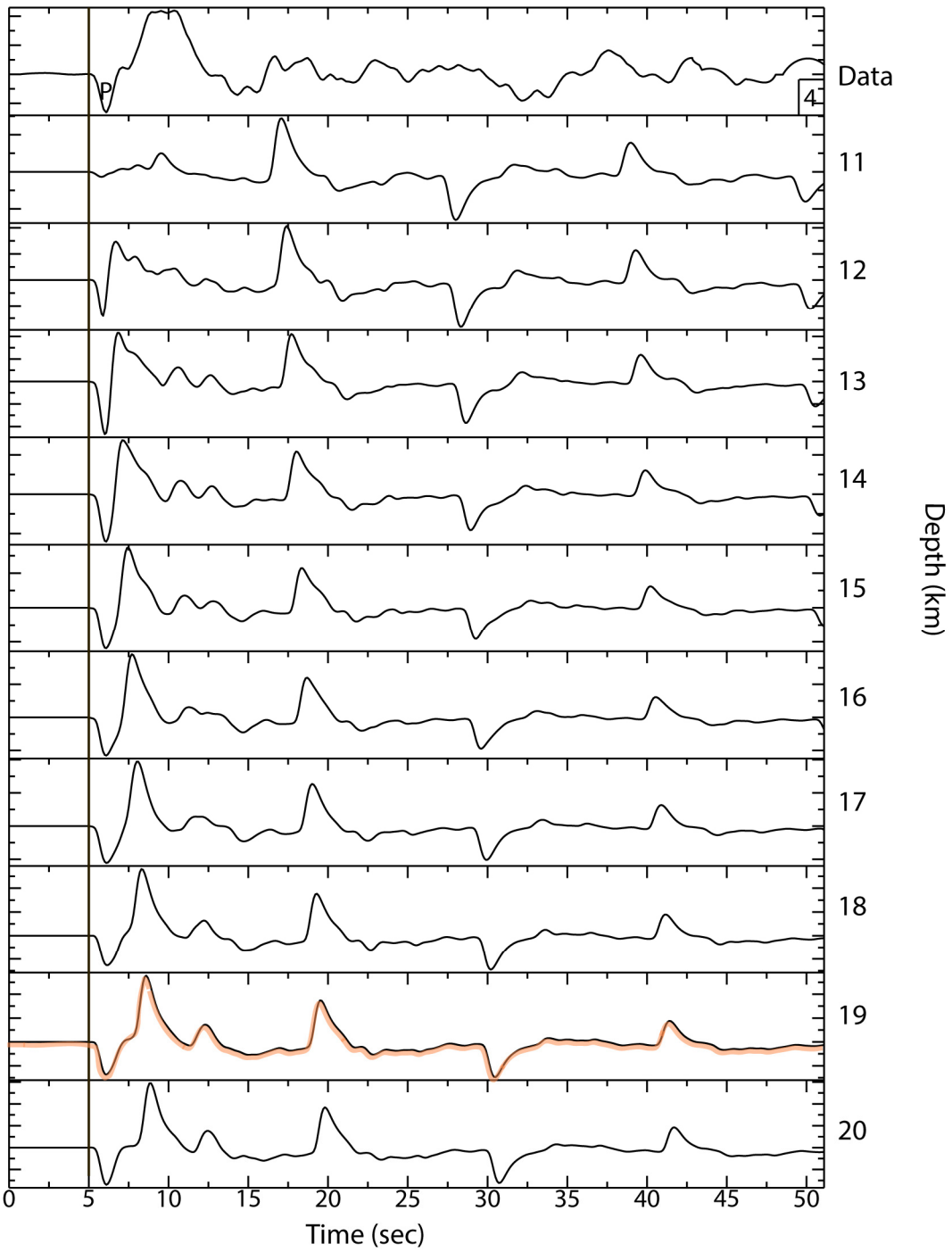

Figure 20. Synthetics for tensional event on 3/24/13. Data for station KBL. Best match for synthetics calculated for a depth of 19km highlighted by orange line.

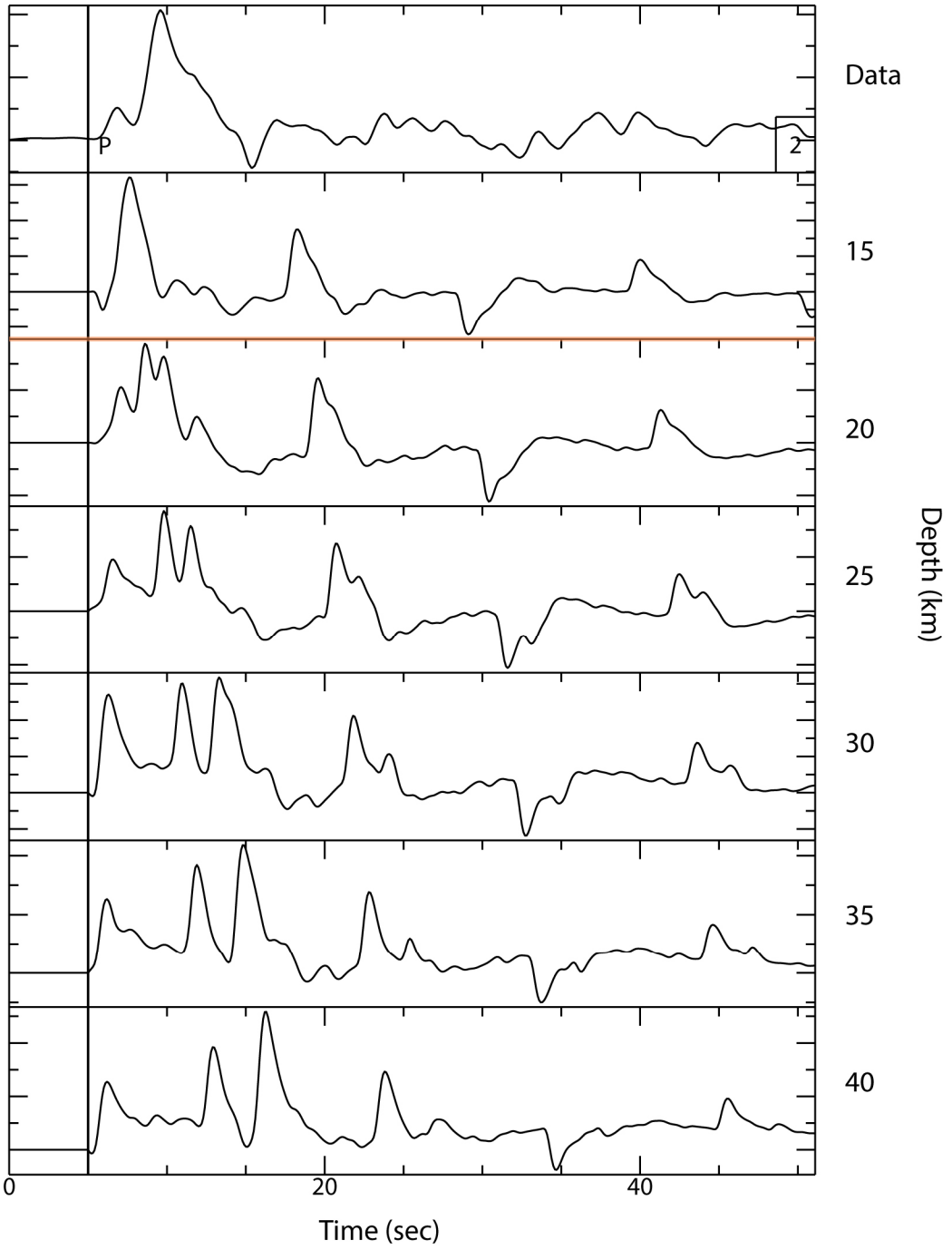

Figure 21. Synthetics for tensional event on 3/24/13. Data from station TLY located at 300° azimuth and 30° distance from event. Best match for synthetics calculated for depths between 15 and 20km (orange line).

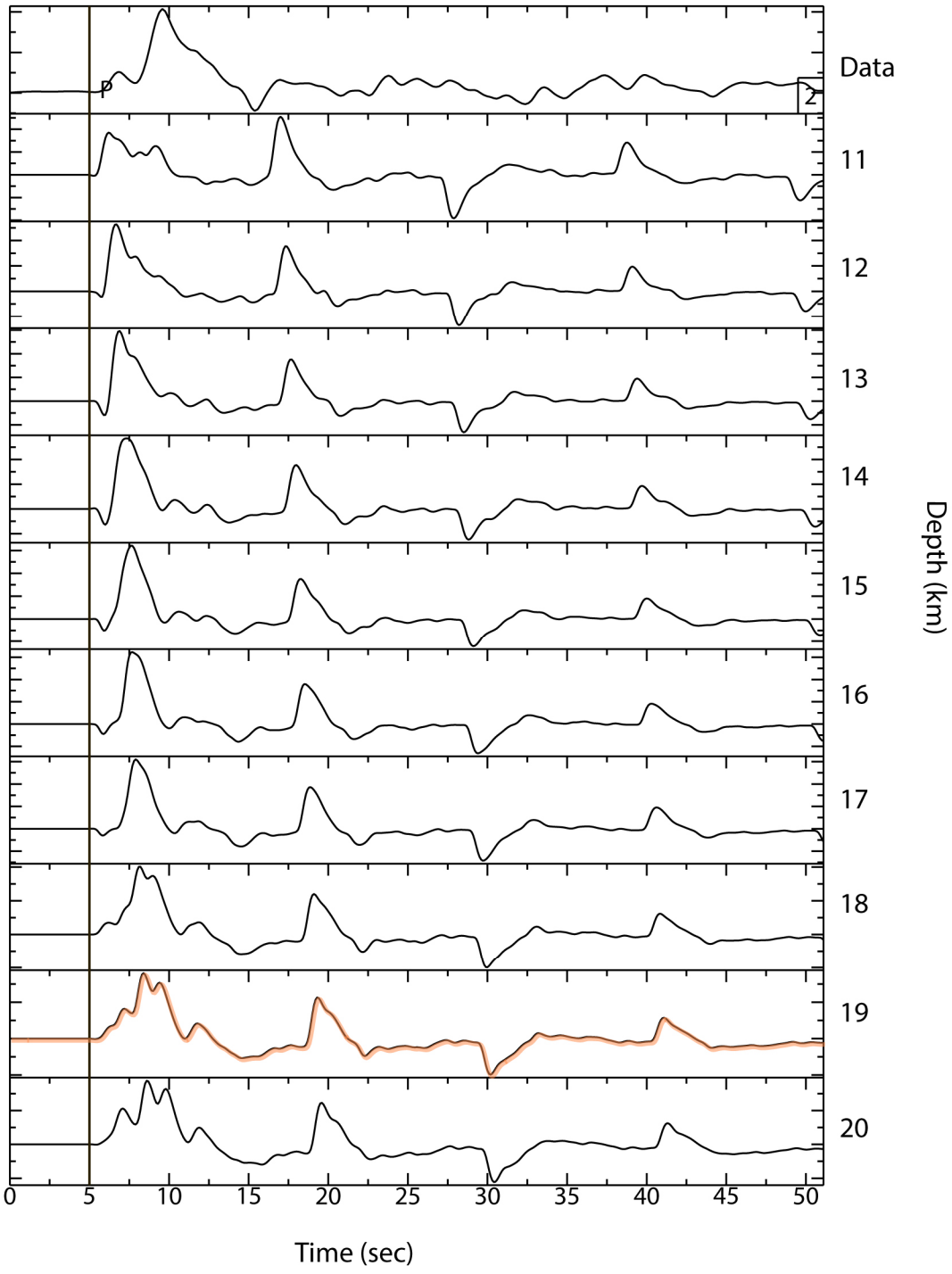

Figure 22. Synthetics for event 3/24/13. Data from station TLY. Best match for synthetics calculated for a depth of 19km highlighted by orange line.

Table 3

Events with Depths from Waveform Analysis

Date	Moment Magnitude (Mw)	Hypocenter Depth (km)	GCMT Depth (km)	Depths from Waveform Analysis (km)	Mechanism
9/10/1990	5.3	23	38	47	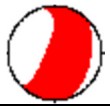
9/5/1994	5.6	33	15	17	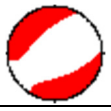
6/19/1995	5.1	33	15	19	
12/4/1995	5.3	42	15	17	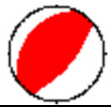
9/13/2004	5.9	8	12	14	
8/10/2005	5.3	31	43	43	
11/19/2006	5.3	12	12	20	
11/28/2006	5.3	10	12	16	
12/7/2006	6.4	16	15	11	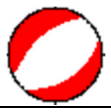
1/17/2009	5.4	22	12	16	
3/24/2013	6.0	8	12	19	

Magnitude, hypocenter and centroid depths, and mechanisms downloaded from Global Centroid Moment Tensor catalog.

P-wave depth phases caused by the presence of the water layer and other interfaces, such as the ocean bottom, in the model are also examined. Without the water layer, the P-waveforms become much more simplified, consisting mainly of the direct wave and secondary reflections off interfaces within the subsurface, most prominently the Earth's surface. With the water layer, several more depth phases are present at larger time separation with the direct P-wave. In both cases, with and without the water layer, the P-waveforms become more complex with depth (Figure 23). Including the water layer in the model is a necessary addition, allowing the synthetics to better match the data.

Three dimensional synthetics were also created using a finite difference technique, as earlier described in the methods chapter, to examine the effect of varying the earthquake depth, but also the differences in synthetics due to varying the horizontal distance from earthquake to trench. Compared to 1-D synthetics, 3-D synthetics allow for more complex P-waveforms that, when compared to data, should show a better match at the correct depth since they include lateral variation in the velocity model as exists in the real Earth, in particular in the shallow subduction zone close to the trench. 1-D synthetics do not exhibit differences in teleseismic P-waveforms with azimuth other than the amplitude and polarity differences produced by the focal mechanism of the earthquake. However, because 3-D synthetic seismograms are calculated to include 3-D variations in the velocity model, differences will be produced in the waveforms as seen at different azimuths. Not all azimuths will show variations. Given the geometries of our 3-D model (a N-S oriented trench) and our source (a 45 degree dipping NS striking normal fault), synthetics for an azimuth of 30° are the same as those for 150° because the model and

earthquake source are identical for both azimuths. Similarly, synthetics for 60° and 330° will be the same for 120° and 210° respectively.

Using 3-D synthetics, the horizontal location of the earthquake, not just depth, could be better determined. Synthetics created for events landwards of the trench, under the trench and oceanwards of the trench each show different depth phases. In the case of an earthquake located oceanwards of the trench, the station at 330° azimuth would record the P-wave interactions with the trench, whereas, the station at 30° azimuth would not. Therefore, synthetics for an event in the outer rise with a station at 330° azimuth show more complex waveforms than a station at 30° azimuth (Figure 24). Conversely, the synthetics for an event landwards of the trench show more complex depth phases at stations with azimuths less than 180° and less complex depth phases at stations greater than 180° (Figure 25-27).

The 3-D synthetics we present in this thesis (Figure 25-27) were created using the same hypothetical tensional earthquake with a N-S striking 45° dipping fault. A hypothetical station located at 35° distance is used for all 3-D synthetic examples. Synthetics for an outer rise event were generated for an earthquake location at 20km oceanward from the trench with the source at a depth of 21km (Figure 25). Synthetics were also created for a source located at 20km landward from the trench at a depth of 21km (Figure 26). The 3-D synthetics generated for an event located 21km beneath the trench show the most complex waveforms and variation with azimuth (Figure 27). Three-dimensional synthetics can also provide more precision into depth determination. Synthetics were generated for an event located 17km below the trench (Figure 28). Synthetics for a source at 13km depth beneath the trench were also created (Figure 29).

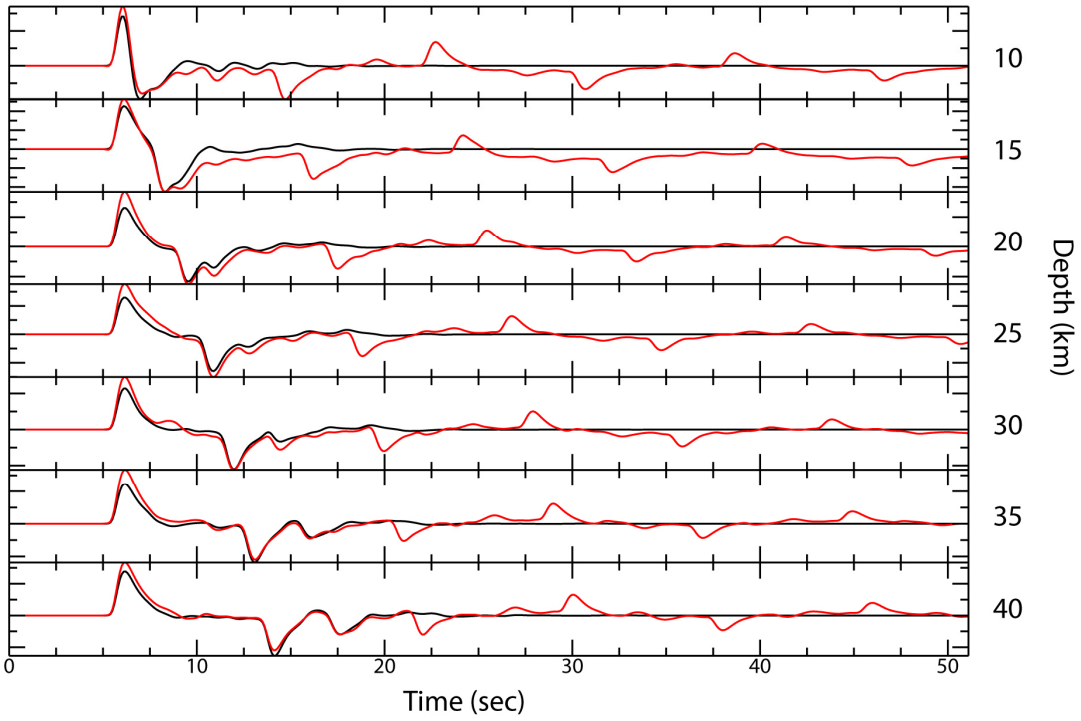

Figure 23. Synthetics calculated for model including water layer (red) and for model without this layer (black) created for a compressional event that occurred on 8/10/2005.

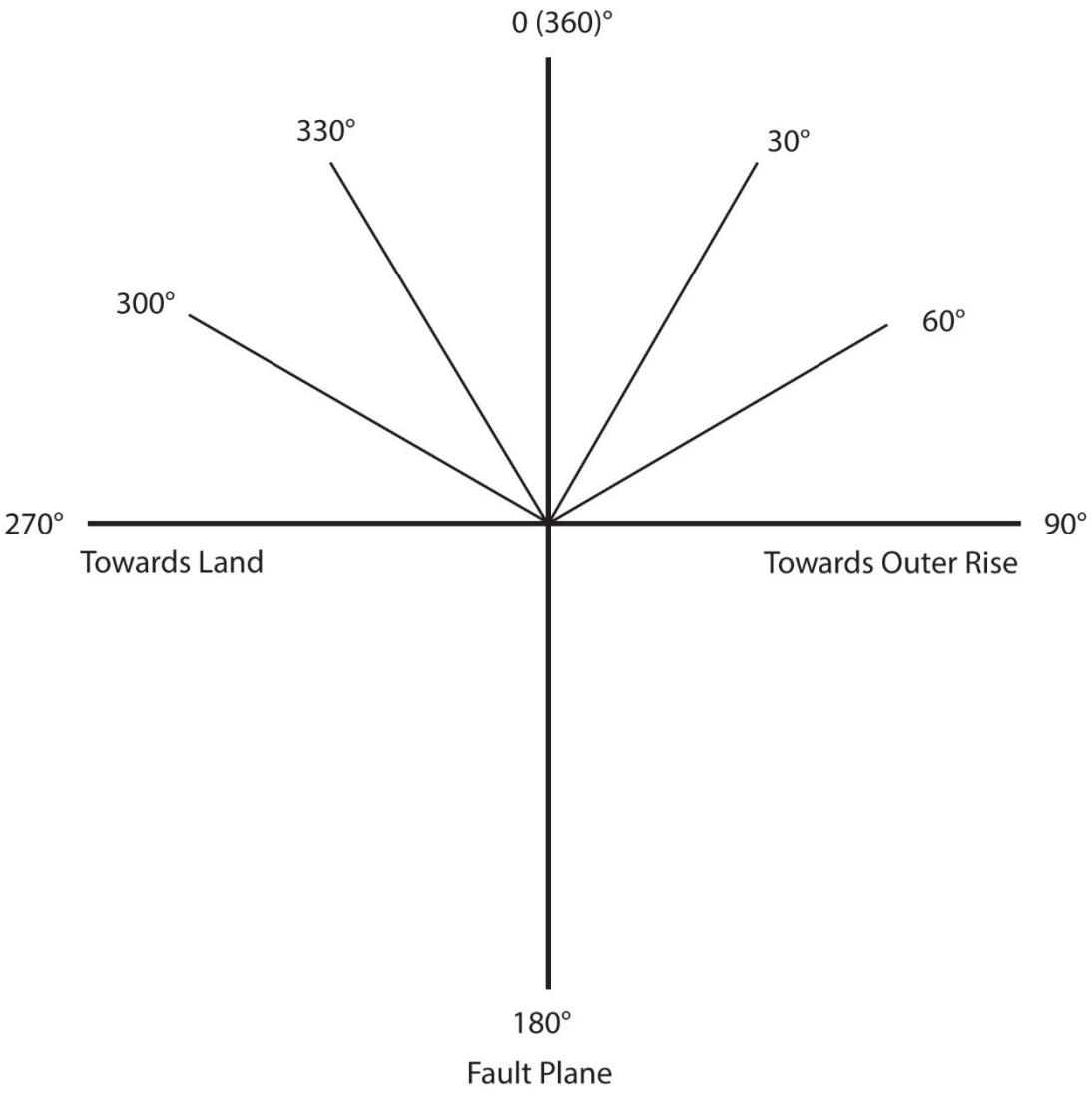

Figure 24. Azimuth diagram for 3-D synthetics. Synthetics at 30° and 150°, 60° and 120°, 330° and 210°, 300° and 240° show identical P-waveforms. Synthetics for 0(360)° and 180° azimuths are also the same.

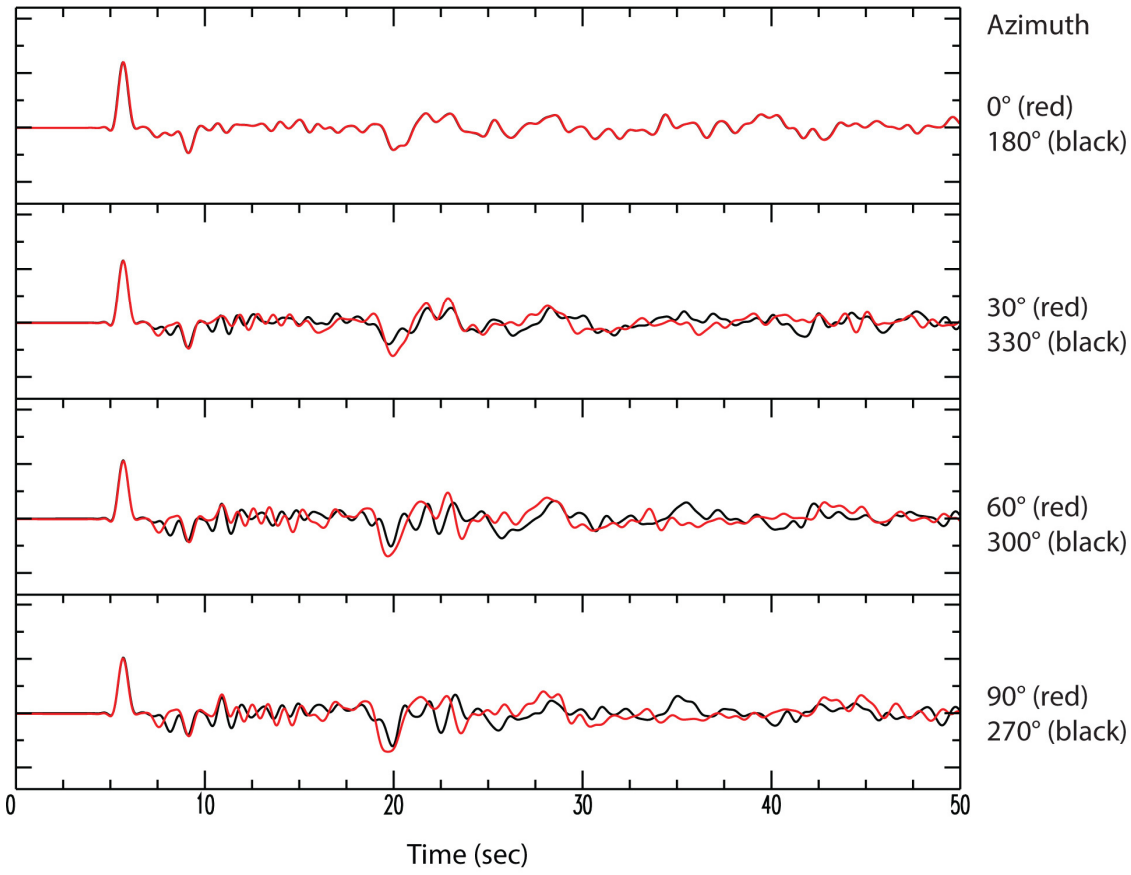

Figure 25. 3D synthetics for a hypothetical tensional earthquake located 20km oceanward of the trench and at 21km depth with a N-S striking 45° dipping fault plane. Hypothetical station located at 35° distance with varying azimuth from fault.

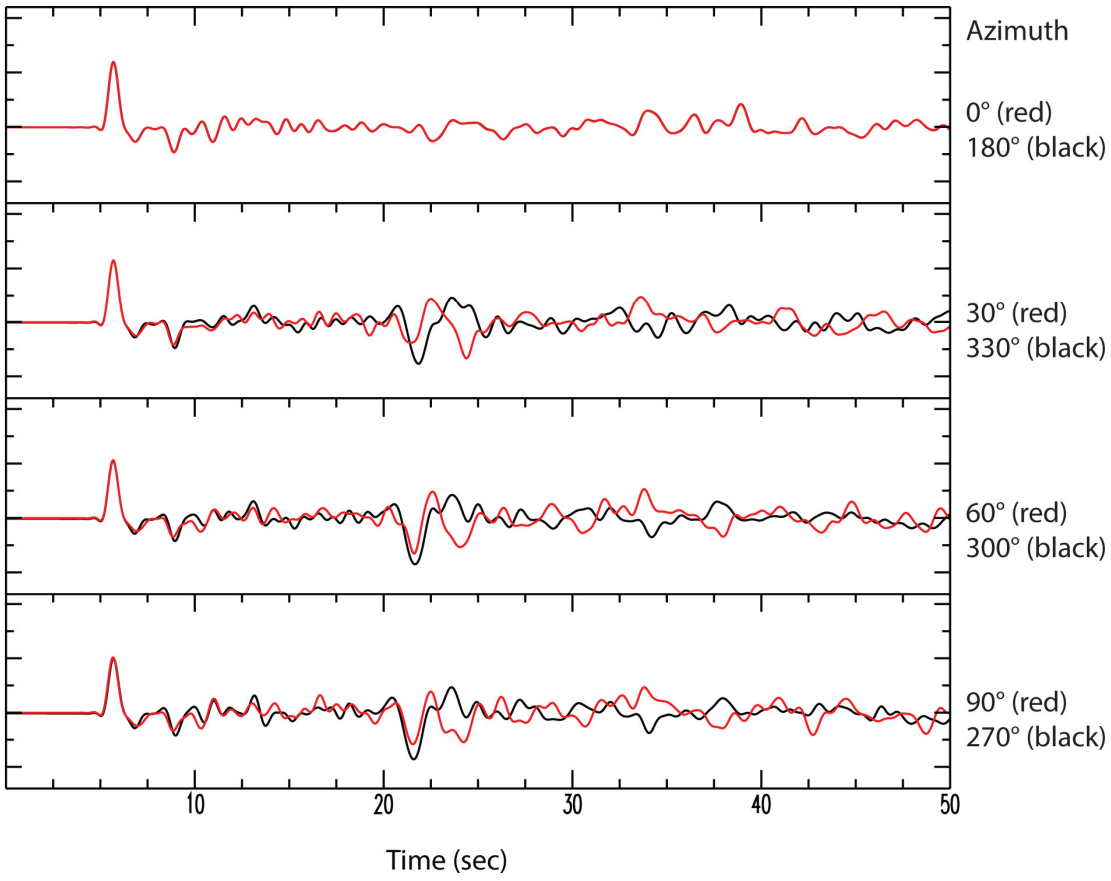

Figure 26. 3D synthetics for a hypothetical tensional earthquake located 20km landward of the trench and at 21km depth with a N-S striking 45° dipping fault plane. Hypothetical station located at 35° distance with varying azimuth from fault.

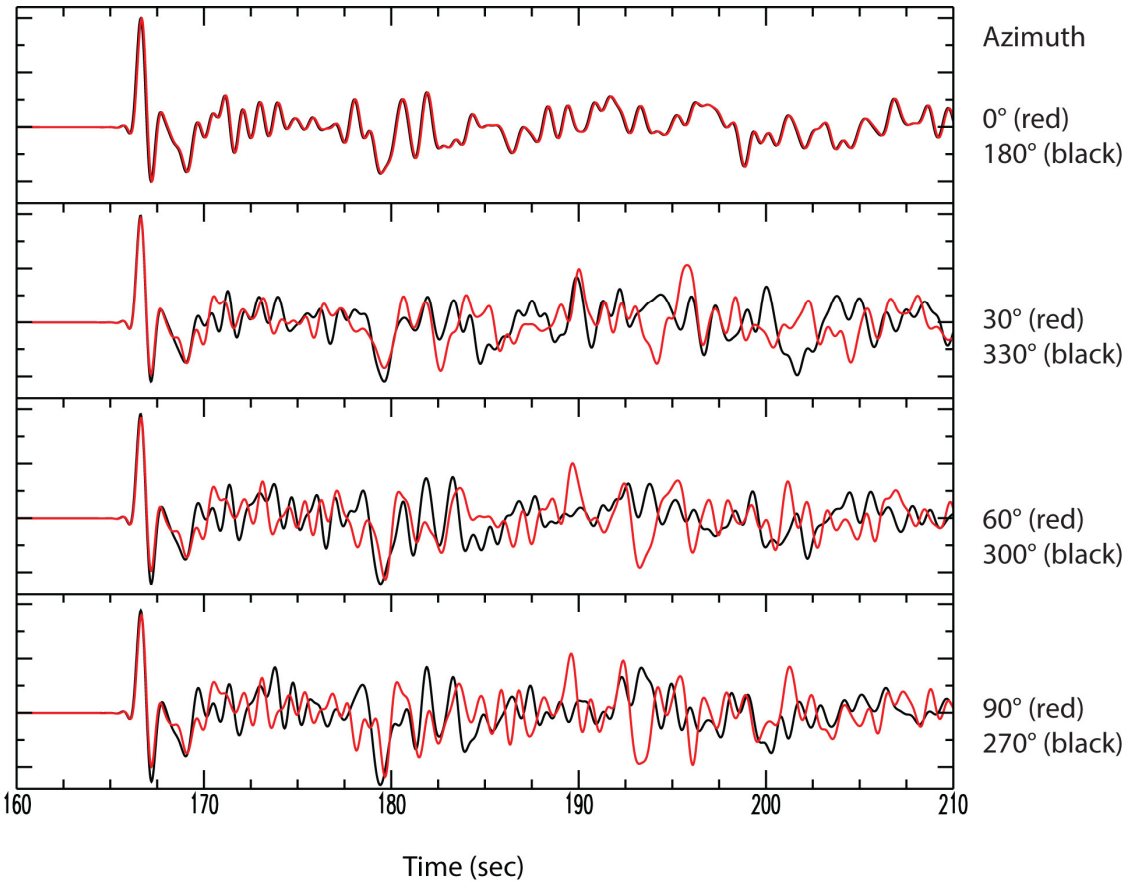

Figure 27. 3D synthetics for a hypothetical tensional earthquake located at 21km depth below the trench with a N-S striking 45° dipping fault plane. Hypothetical station located at 35° distance with varying azimuth from fault.

Azimuthal variation in data shows similarities to 3-D synthetics; an example of such azimuthal variation is shown in Figure 30. However, the data shows a longer wavelength P-waveforms with depth phases occurring later in the seismogram. The data shown in Figure 30 likely was generated by an earthquake with different depth than that was used to generate synthetics in Figures 25-27. From these preliminary results, it appears a direct comparison of recorded waveforms and 3-D synthetics for the purpose of detailed horizontal and vertical location may not be feasible for the current dataset within the time limits of this thesis research project.

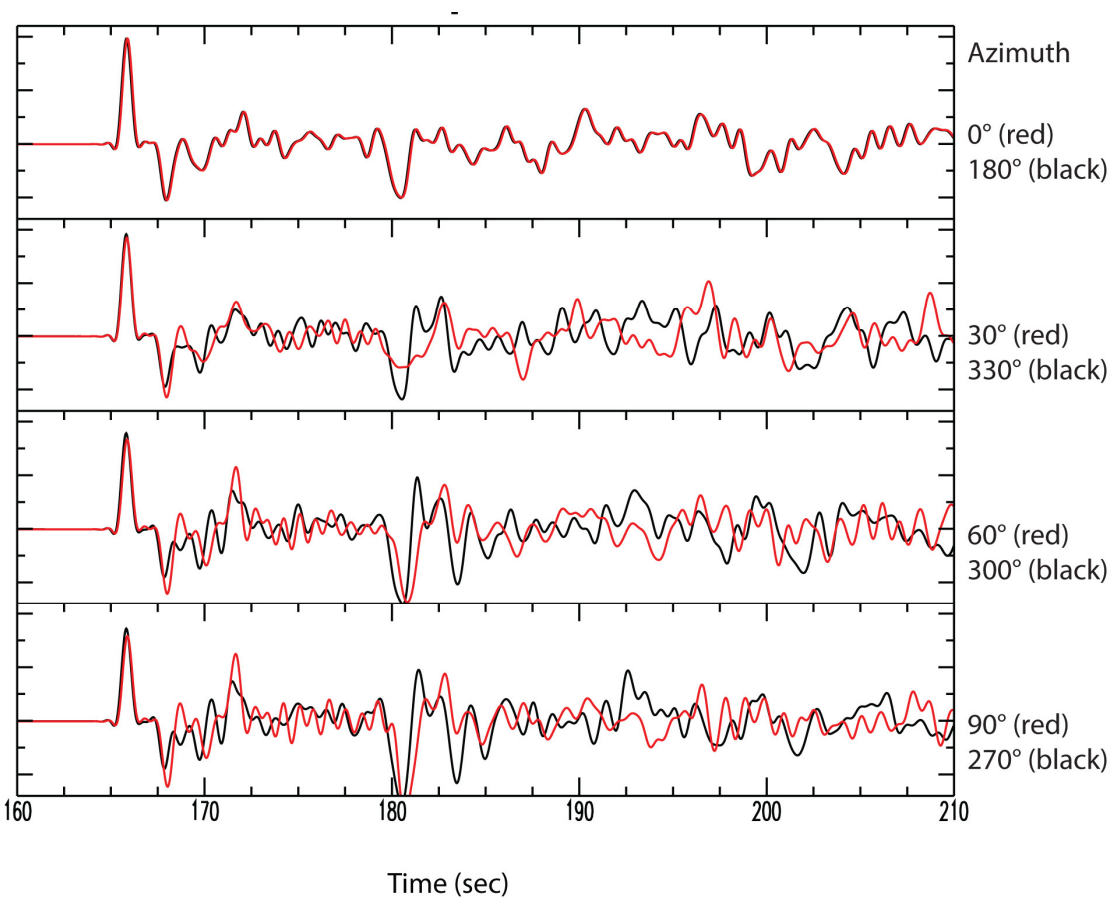

Figure 28. 3D synthetics for a hypothetical tensional earthquake located at 17km depth under the trench with a N-S striking 45° dipping fault plane. Hypothetical station located at 35° distance with varying azimuth from event.

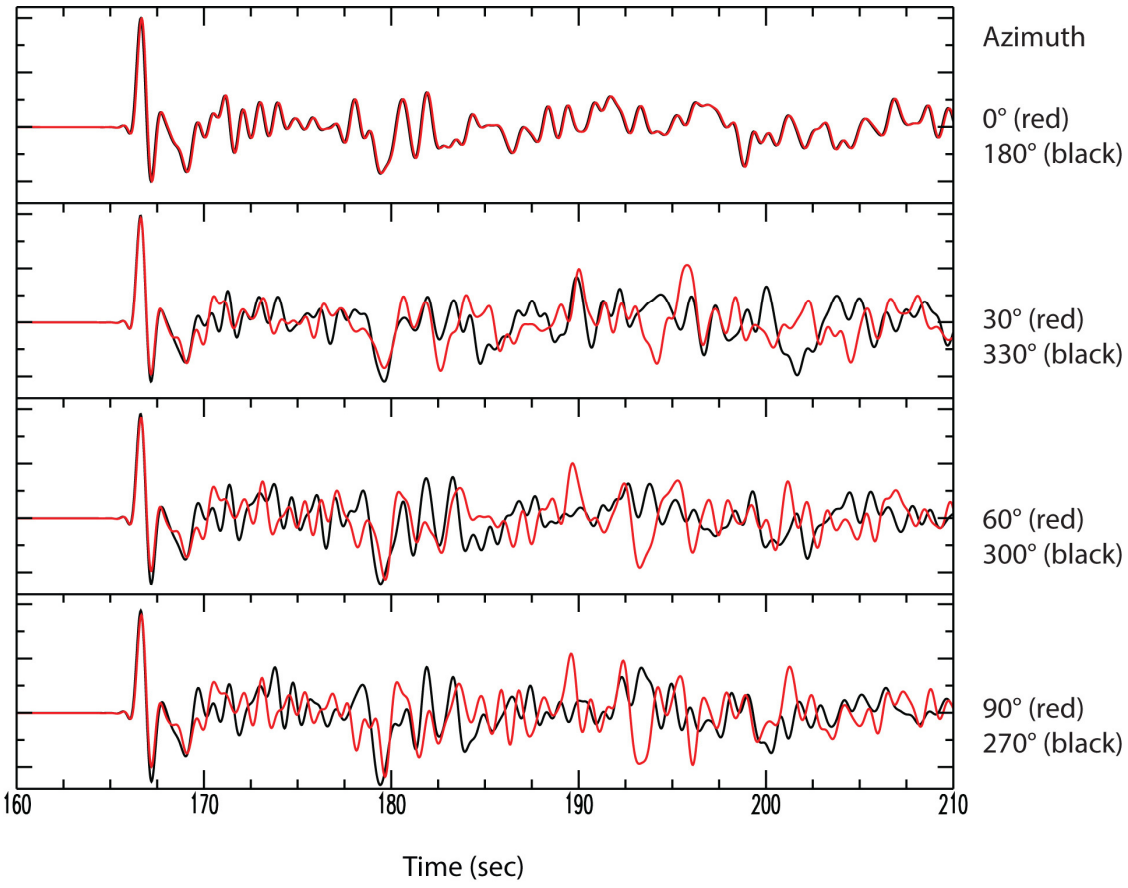

Figure 29. 3D synthetics for a hypothetical tensional earthquake located at 13km depth under the trench with a N-S striking 45° dipping fault plane. Hypothetical station located at 35° distance with varying azimuth from fault.

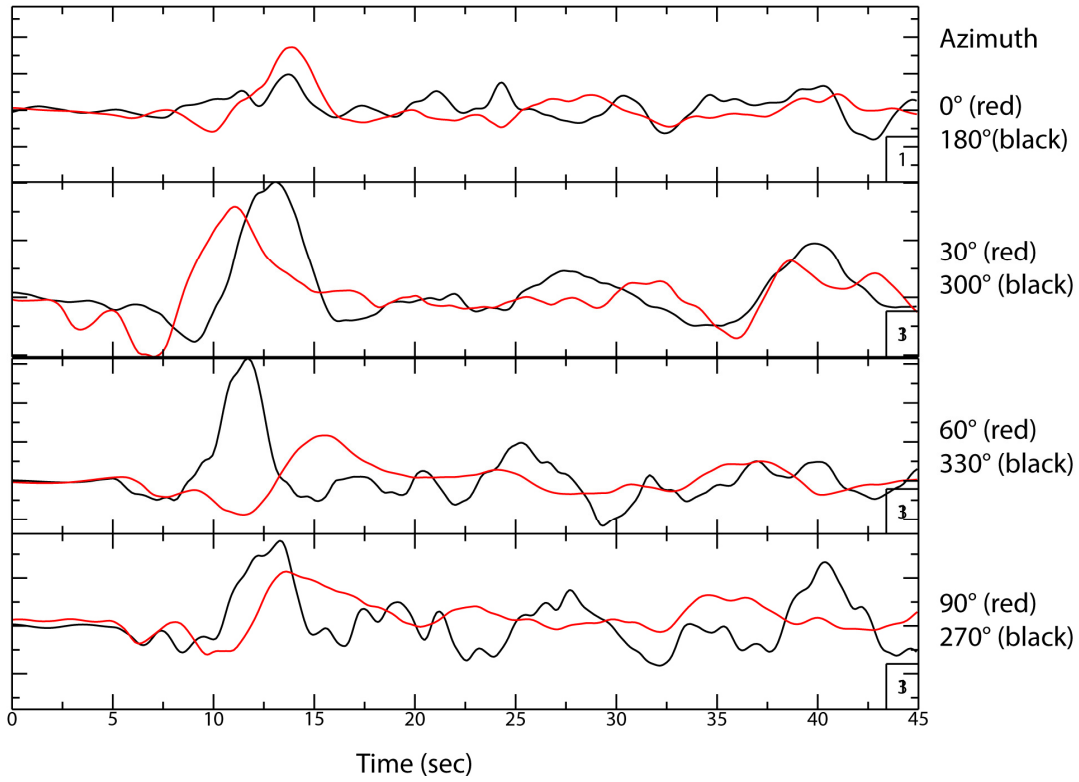

Figure 30. Azimuth comparison for tensional event on 12/7/2006 with a fault dip of 45 striking NE-SW. Station ALE used for 0° azimuth. Station PATS used for 180° azimuth. Station PKME used for 30° azimuth. Station TRI used for 330° azimuth. Station EUO used for 60° azimuth. Station KZA used for 300°azimuth. Station MA06 used for 90° azimuth. Station ENH used for 270° azimuth.

CHAPTER FOUR

DISCUSSION

The depths we determined using waveform analysis for selected outer rise compressional and tensional events are generally larger than the reported Global Centroid Moment Tensor (GCMT) depths (Figure 31). The GCMT inversion depth is often held fixed at 10 or 15km due to instable inversions (Konstantinou & Rontogianni, 2011; Ekström et al., 2012). By generating synthetic seismograms for a range of depths and comparing them to recorded waveform data for teleseismic P-waves, we have more precisely determined depths for these events.

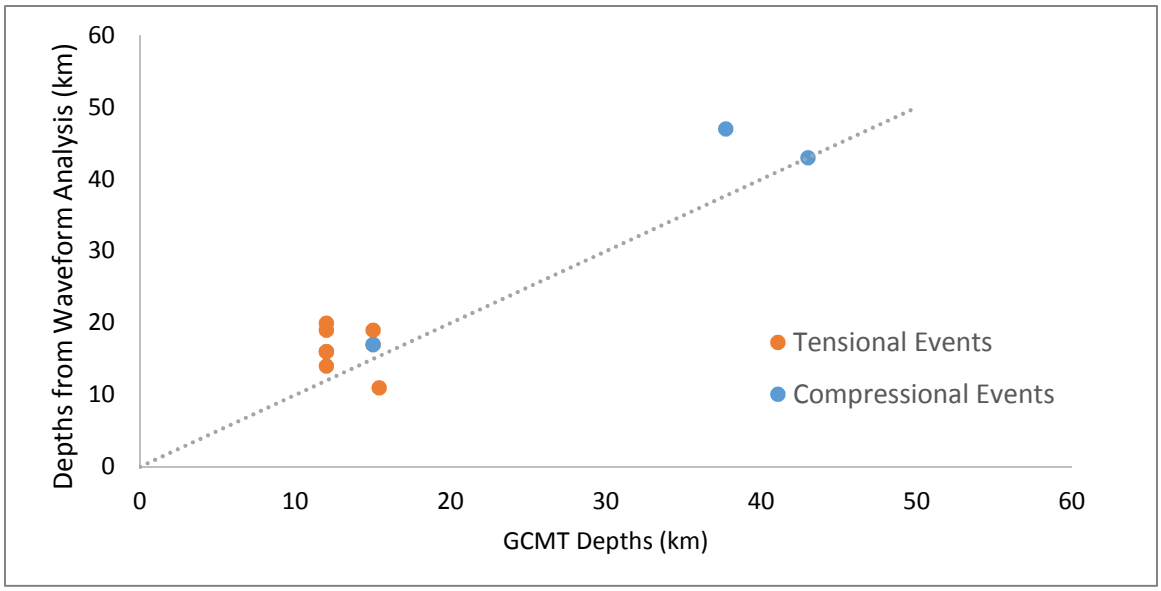

Figure 31. Comparison between centroid depths determined by waveform analysis and corresponding depths from GCMT catalog. Compressional events colored blue, tensional events colored orange. Dashed line represents computed depths equaling GCMT depths.

A compressional event on 8/10/2005 was found to have the same depth as suggested by GCMT.Similarly, a tensional event on 12/7/2006 was found to have a shallower depth than presented by GCMT. The remaining events were found to have larger depths than the GCMT centroid depths. The shallow compressional outlier event, which occurred on 12/4/1995, was found using waveform analysis to have a similar shallow depth as suggested by the GCMT catalog.

We also show a comparison of our depths with the hypocenters from the GCMT catalog in Figure 32. Although hypocentral depths are commonly determined from body waveforms, such as the teleseismic P-waves we used in this study, our results indicate the GCMT depths are generally better determined, although their analysis uses long period waveforms (Figure 32). In particular, one event with a large difference between hypocentral and GCMT depths, namely 42.2 km and 15 km, was shown by our waveform analysis to have a depth of 17 km, much closer to the GCMT depth.

The GCMT catalog provides error estimates for its centroid depths. We find that the GCMT depths are reasonably well determined for these events, as they match our depths within 10km. The error provided is generally zero which is much smaller than the difference between our improved depths and the centroid depths given by GCMT (Table 4) and therefore does not appear to give a realistic indication of the true error in this measurement. The average difference between the centroid depths and depths determined from waveform analysis is 3.4km. Similarly, the maximum deviation between the GCMT error and difference between the centroid and improved depths is 8km for the tensional event on 11/19/2006.

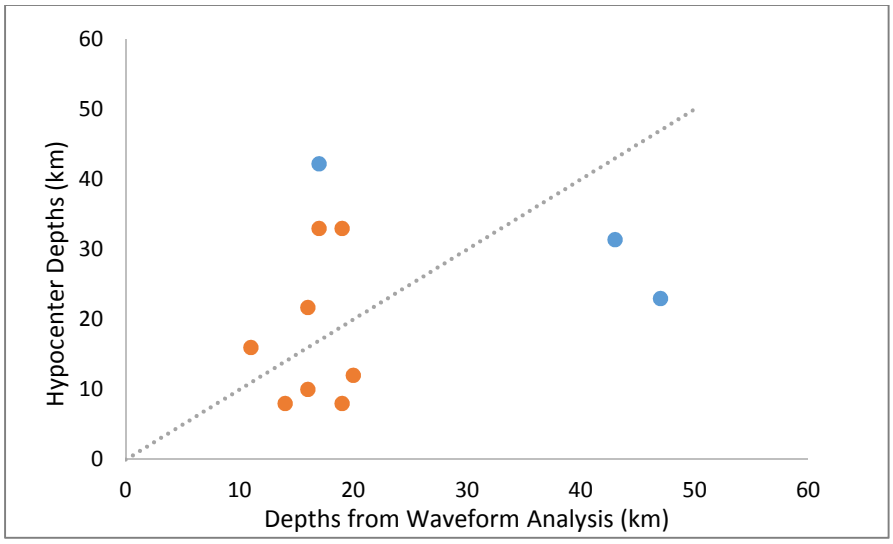

Figure 32. Comparison between hypocenter depths from GCMT catalog and depths determined by waveform analysis. Compressional events colored blue, tensional events colored orange.

Table 4

GCMT and Improved Depths for Selected Events

Date	GCMT Depth (km)	Depth Determined from Waveform Analysis (km)	GCMT Error (km)	Centroid and Improved Difference (km)
9/10/1990	37.7	47	4.6	9.3
9/5/1994	15	17	0	2
6/19/1995	15	19	0	4
12/4/1995	15	17	0	2
9/13/2004	12	14	0	2
8/10/2005	43	43	0	0
11/19/2006	12	20	0	8
11/28/2006	12	16	0	4
12/7/2006	15.4	11	0.1	-4.4
1/17/2009	12	16	0	4
3/24/2013	12	19	0	7

GCMT Error and Difference between Centroid Depths and Depths Determined from Waveform Analysis

Most of the events analyzed with waveform analysis have positive depth differences from the GCMT depths, suggesting a possible systematic bias in their analysis (Figure 33).

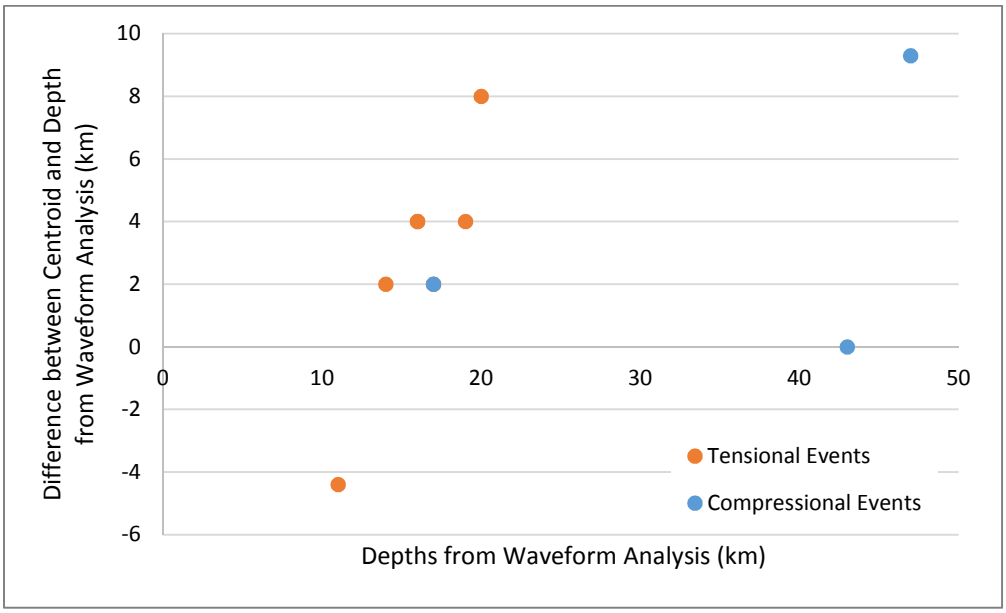

Figure 33. Comparison between depths from waveform analysis and difference between centroid depths and depths from waveform analysis.

To examine the spatio-temporal relationships between the outer rise and large interface earthquakes and relate these observations to the seismic cycle, we plot these events as a function of date and depth (Figure 34). The Kuril outer rise has experienced limited seismicity between magnitude 5.1 and 6.4 prior to 1996. Four out of eleven selected outer rise events occur between 1990 and 1996. The remaining seven occur from 2004 to 2013 (Figure 35). A majority of large interface events, greater than magnitude 7, presented occur before 1996. However, outer rise events preceding 1996 do not exceed magnitude 6. Along with an increased number of outer rise events, the magnitudes of the outer rise events also increased. Most notably two large outer rise events, one tensional

M8.1 and one compressional M7.3, occurred in the region. Similar to events prior to 1996, tensional events post 2005 occurred at depths shallower than 20km. Both compressional events, however, take place deeper than 40km. 2004 to 2013 (Figure 35).

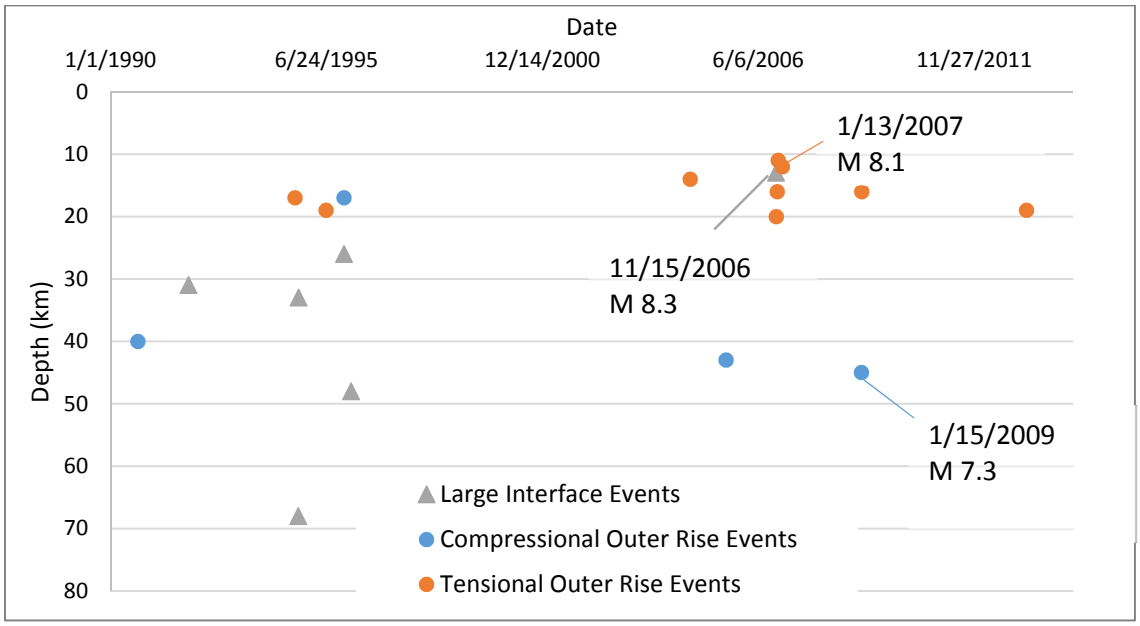

Figure 34. Interface and outer rise events plotted by date and depth. Large interface events, greater than magnitude 7, plotted as gray triangles (depths from GCMT catalog), compressional outer rise events plotted as blue circles, tensional outer rise events plotted as orange circles. Dates and magnitudes are provided for two large outer rise events, depths are provided by the GCMT catalog.

Along with an increased number of outer rise events, the magnitudes of the outer rise events also increased. Most notably two large outer rise events, one tensional M8.1 and one compressional M7.3, occurred in the region. Similar to events prior to 1996, tensional events post 2005 occurred at depths shallower than 20km. Both compressional events, however, take place deeper than 40km. 2004 to 2013 (Figure 35).

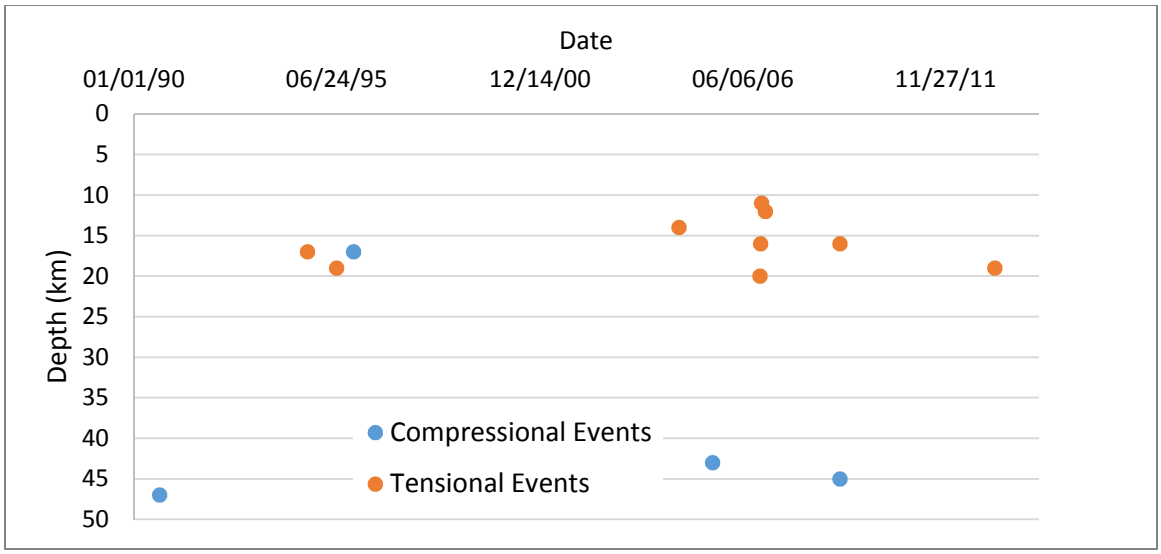

Figure 35. Outer rise events plotted as a function of depth and date. Blue circles represent compressional events. Orange circles represent tensional events.

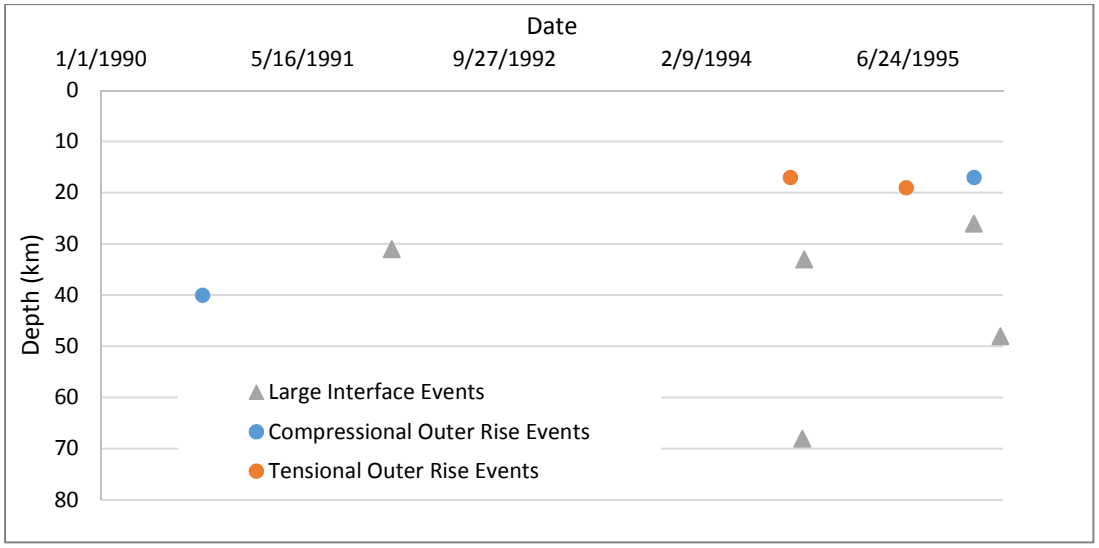

Figure 36. Temporal evolution of earthquakes in the Kuril region from 1/1/1990 to 2/7/1996 showing large interface along with compressional and tensional events.

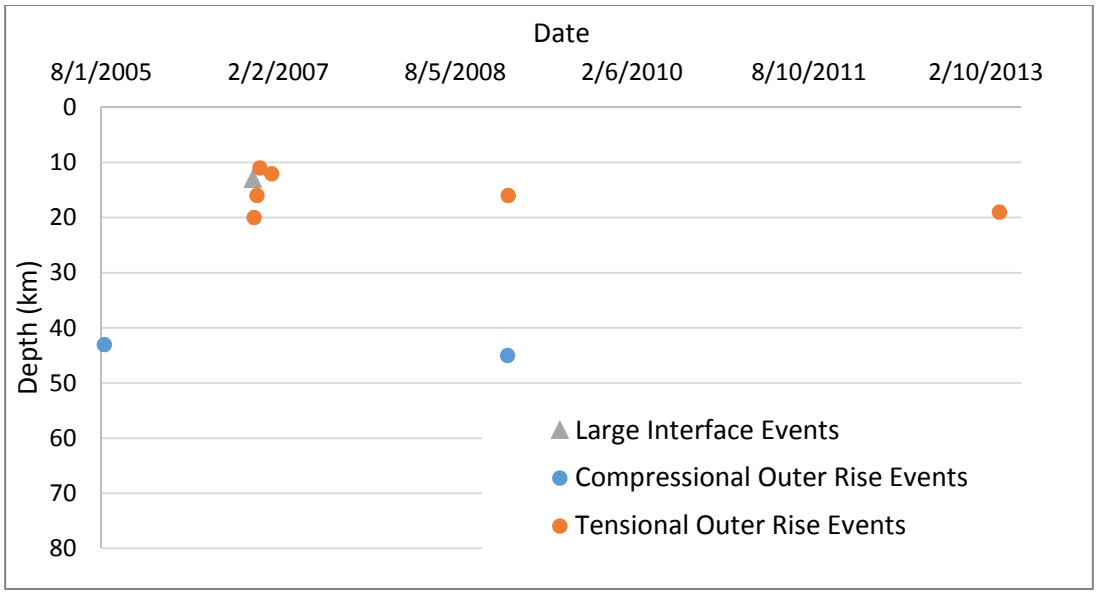

Figure 37. Temporal evolution of earthquakes in the Kuril region from 8/1/2005 to 6/1/2013 showing large interface along with compressional and tensional events.

To be able to relate these observations to the seismic cycle, we need to divide the outer rise events into subsets. Some of these earthquakes are located in the outer rise area offshore of the rupture area of the 2006 interface event, and thus reflect the post-interface event part of the seismic cycle. Others are located in the outer rise to the North and South of this rupture area, where large interface events occurred more than 50 years ago. Therefore, these events are indicative of a different part of the seismic cycle and therefore we will show them in separate graphs.

Outer rise events located near the M8.3 11/15/2006 rupture area are primarily tensional outer rise events occurring after the main interface event (Figure 38). Based on this dataset, one consistent neutral stress surface between compressional and tensional events may be drawn at a depth between 20 and 40 km. No change in neutral surface depth before and after the interface event is required by the data. Based on the simple

model by Liu and McNally (1993), however, after a large interface event, the neutral surface defining depths to outer rise events should shift causing deeper tensional events and eliminating compressional outer rise events. A M7.3 compressional event that occurred on 1/15/2009 after the 2006 interface event also indicates that the regional stress along the Kuril trench is more complex than suggested by the Liu and McNally model. Compressional events that occur at any time during the seismic cycle may, however, be explained by in-plane compression associated with increased stress concentrations along the subduction zone due to trench compression or strength heterogeneities along the trench (Mueller et al., 1995). Another possible explanation for the occurrence of a compressional outer rise event shortly after a larger interface event would be through the process of dynamic stress triggering (Kilb et al., 2000).

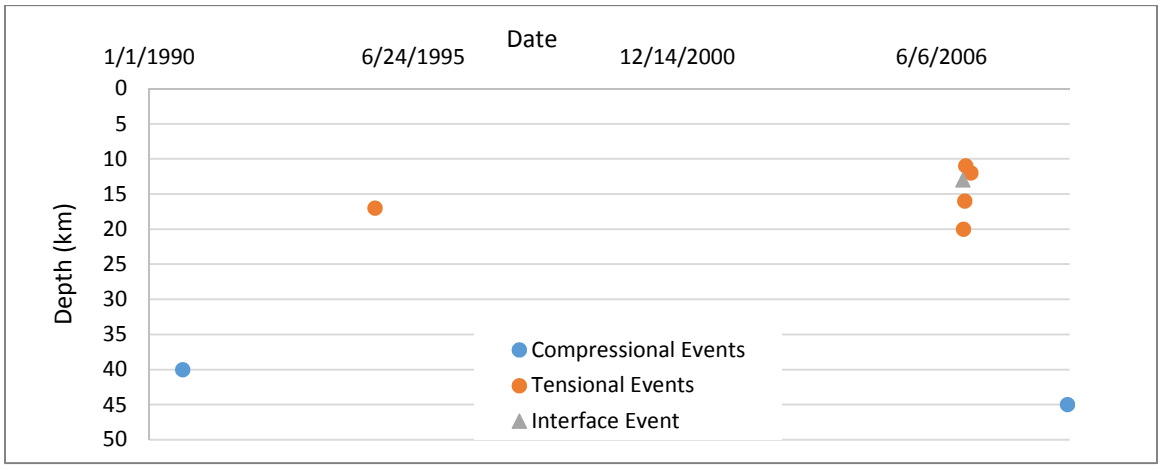

Figure 38. Outer rise events within the 11/15/2006 rupture area. Compressional outer rise events plotted at blue circles, tensional outer rise events plotted as orange circles and the interface event plotted as a gray triangle.

The outer rise events located south of the 2006 rupture area contradict the simple stress model (Figure 39). A M 5.1 tensional event occurred on 6/19/1995 prior to a magnitude 7.9 interface event on 12/3/1995. A M 5.3 compressional event occurred the following day. Assuming the Liu and McNally (1993) stress model, compressional events should only occur prior to a large interface event. Compressional events post interface event can only be explained by a complex model, such as suggested by Mueller et al. (1995). In addition to allowing compressional and tensional events at any time during the seismic cycle, large interface events do not occur temporally near large outer rise events under the more complex model (Mueller et al., 1995). More interface events compared to outer rise events occurred prior to 1996, whereas, more and larger magnitude outer rise events occurred relative to interface events after 2005.

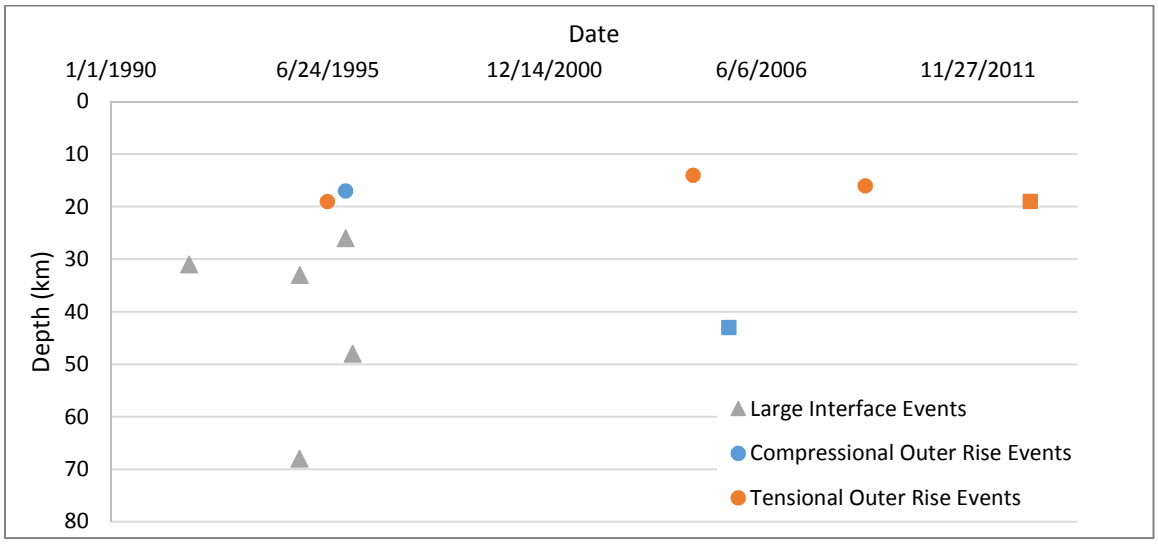

Figure 39. Outer rise events outside of the 11/15/2006 rupture area. Compressional outer rise events plotted as blue circles (southern) and squares (northern). Tensional outer rise events plotted as orange circles (southern) and squares (northern). Interface events plotted as gray triangles.

Our results for both the 2006 rupture area and the surrounding regions, suggest that interface events may have a negligible effect on the state of stress in the outer rise and that the bending stresses dominate. Large strength heterogeneities are required to explain the observed occurrence (both in time and space) of compressional and tensional outer rise quakes. To be able to carry out a more detailed analysis of the spatio-temporal relationships between interface and outer rise seismicity, a larger dataset would be required. To this end, the waveform analysis would have to be applied to smaller magnitude earthquakes. Earthquakes smaller than 5 magnitude would require more processing to isolate the event signal from noise. With events under magnitude 5.5, only a few stations were usable; the removal of instruments response and integration to displacement createdunusable waveforms. To facilitate the use of smaller magnitude earthquakes, seismograms may be analyzed in the velocity domain, instead of in displacement. However, since velocity records are dominated by shorter period signal, they are also more susceptible to 3-D short wavelength structural variations, which complicates their interpretation and comparison with synthetics. Events with magnitudes greater than 7 may cause higher amplitude waves than a seismogram can record leaving no usable information about initial P-wave and subsequent depth phases. At these greater magnitudes, one can also no longer assume a point source approximation, as we have done in the calculation of the synthetics, since the finiteness of the rupture may have a significant effect on the waveforms.

p

CHAPTER FIVE

CONCLUSIONS

We have analyzed 11 outer rise earthquakes in the central part of the Kuril subduction zone by comparing 1-D synthetic seismograms of teleseismic P-waves with recorded waveform data to determine improved hypocentral depths. These more accurate outer rise event depths provide insight into the seismic cycle and the state of stress in the outer rise and its temporal relationship to large proximal interface events. Depths analyzed with waveform analysis are more accurate than those determined by routine processing methods, such as the Global Centroid Moment Tensor catalog. From our comparison of the routine catalog results with our waveform analysis, we have determined that the GCMT centroid depths are more accurate than the routinely determined hypocenter depths, with centroid depths less than 10km from our depths determined by waveform analysis.

Our preliminary results from the calculation of 3-D synthetic seismograms suggest that they may be used to determine even more precise depths to events and lateral location relative to the trench. However, the quality and quantity of the current waveform data is not adequate for an in-depth analysis.

Our results indicate that some compressional and tensional outer rise events occur in close proximity in space and time. We do not observe any change in the depth of the neutral stress surface due to the occurrence of large interface events. Several compressional events occur directly following large nearby interface events. These observations suggest that the simple model of Liu and McNally (1993), in which stress

transfer due to interface events significantly modulates the outer rise state of stress, and thus seismicity, is not a good fit with our data. A more complicated stress model, which incorporates large stress heterogeneities or dynamic stress triggering, is required by our data.

REFERENCES

Ammon, C. J., Kanamori, H., & Lay, T. (2008). A great earthquake doublet and seismic stress transfer cycle in the central Kuril Islands. *Nature, 451*(7178), 561-565.

Astiz, L., Lay, T., & Kanamori, H. (1988). Large intermediate-depth earthquakes and the subduction process. *Physics of the Earth and Planetary interiors, 53*(1), 80-166.

Christensen, D. H., & Ruff, L. J. (1983). Outer-rise earthquakes and seismic coupling. *Geophysical Research Letters, 10*(8), 697-700.

Christensen, D. H., & Ruff, L. J. (1988). Seismic coupling and outer rise earthquakes. *Journal of Geophysical Research: Solid Earth (1978–2012),93*(B11), 13421-13444.

Crotwell, H. P., Owens, T. J., & Ritsema, J. (1999). The TauP Toolkit: Flexible seismic travel-time and ray-path utilities, *Seismological Research Letters, 70*, 154–160.

Di Giacomo, D., Storchak, D. A., Safronova, N., Ozgo, P., Harris, J., Verney, R., & Bondár, I. (2014). A New ISC Service: The Bibliography of Seismic Events. *Seismological Research Letters*, *85*(2), 354-360.

Dziewonski, A. M., Chou, T. A., & Woodhouse, J. H. (1981). Determination of earthquake source parameters from waveform data for studies of global and regional seismicity. *Journal of Geophysical Research: Solid Earth (1978–2012)*,*86*(B4), 2825-2852.

Ekström, G., Nettles, M., & Dziewoński, A. M. (2012). The global CMT project 2004–2010: centroid-moment tensors for 13,017 earthquakes. *Physics of the Earth and Planetary Interiors*, *200*, 1-9.

Geist, E., Kirby, S., Ross, S., & Darnell, P. Samoa Disaster Highlights Danger of Tsunamis Generated from Outer-Rise Earthquakes. Dec. 2009. Retrieved October 21, 2012 from http://soundwaves.usgs.gov/2009/12/research.html.

Gnibidenko, H., Bykova, T. G., Veselov, O. V., Vorobiev, V. M., & Svarichevsky, A. S. (1981). *The Tectonics of the Kuril-Kamchatka Deep-Sea Trench* (pp. 249-285). American Geophysical Union.

Hanks, T. C. (1971). The Kuril trench-Hokkaido rise system: Large shallow earthquakes and simple models of deformation. *Geophysical Journal International, 23*(2), 173-189.

Hyndman, R. D., Yamano, M., & Oleskevich, D. A. (1997). The seismogenic zone of subduction thrust faults. *Island Arc, 6*(3), 244-260.

Igarashi, T., Matsuzawa, T., & Hasegawa, A. (2003). Repeating earthquakes and interplate aseismic slip in the northeastern Japan subduction zone. *Journal of Geophysical Research: Solid Earth (1978–2012), 108*(B5).

International Seismological Centre, On-line Event Bibliography, Retrieved December 1, 2013 from http://www.isc.ac.uk/event_bibliography, Internatl. Seis. Cent., Thatcham, United Kingdom, 2014.

Jackson, J., McKenzie, D. A. N., Priestley, K., & Emmerson, B. (2008). New views on the structure and rheology of the lithosphere. *Journal of the Geological Society*, *165*(2), 453-465.

Jiao, W., Silver, P. G., Fei, Y., & Prewitt, C. T. (2000). Do intermediate-and deep-focus earthquakes occur on preexisting weak zones? An examination of the Tonga subduction zone. *Journal of Geophysical Research: Solid Earth (1978–2012), 105*(B12), 28125-28138.

Kilb, D., Gomberg, J., & Bodin, P. (2000). Triggering of earthquake aftershocks by dynamic stresses. *Nature*, *408*(6812), 570-574.

Konstantinou, K. I., & Rontogianni, S. (2011). A Comparison of Teleseismic and Regional seismic Moment Estimates in the European-Mediterranean Region.*Seismological Research Letters*, *82*(2), 189.

Lay, T., Ammon, C. J., Kanamori, H., Kim, M. J., & Xue, L. (2011). Outer trench-slope faulting and the 2011 Mw 9.0 off the Pacific coast of Tohoku Earthquake. *Earth, planets and space, 63*(7), 713-718.

Lay, T., Astiz, L., Kanamori, H., & Christensen, D. H. (1989). Temporal variation of large intraplate earthquakes in coupled subduction zones. *Physics of the earth and planetary interiors, 54*(3), 258-312.

Lay, T., Kanamori, H., Ammon, C. J., Hutko, A. R., Furlong, K., & Rivera, L. (2009). The 2006–2007 Kuril Islands great earthquake sequence. *Journal of Geophysical Research: Solid Earth (1978–2012), 114*(B11).

Liu, X., & McNally, K. C. (1993). Quantitative estimates of interplate coupling inferred from outer rise earthquakes. *Pure and Applied Geophysics, 140*(2), 211-255.

Moore, J. C., & Saffer, D. (2001). Updip limit of the seismogenic zone beneath the accretionary prism of southwest Japan: An effect of diagenetic to low-grade metamorphic processes and increasing effective stress. *Geology, 29*(2), 183-186.

Mueller, S., Spence, W., & Choy, G. L. (1996). Inelastic models of lithospheric stress-II: Implications for outer-rise seismicity and dynamics. *Geophysical Journal International*, *125*(1), 54-72.

Nanayama, F., Satake, K., Furukawa, R., Shimokawa, K., Atwater, B. F., Shigeno, K., & Yamaki, S. (2003). Unusually large earthquakes inferred from tsunami deposits along the Kuril trench. *Nature, 424*(6949), 660-663.

Obana, K., Fujie, G., Takahashi, T., Yamamoto, Y., Nakamura, Y., Kodaira, S., & Shinohara, M. (2012). Normal-faulting earthquakes beneath the outer slope of the Japan Trench after the 2011 Tohoku earthquake: Implications for the stress regime in the incoming Pacific plate. *Geophysical Research Letters,39*(7).

Okamoto, T. (1994). Teleseismic synthetics obtained from 3-D calculations in 2-D media. *Geophysical Journal International*, *118*(3), 613-622.

Pacheco, J. F., Sykes, L. R., & Scholz, C. H. (1993). Nature of seismic coupling along simple plate boundaries of the subduction type. *Journal of Geophysical Research: Solid Earth (1978–2012), 98*(B8), 14133-14159.

Pitarka, A. (1999). 3D elastic finite-difference modeling of seismic motion using staggered grids with nonuniform spacing. *Bulletin of the Seismological Society of America, 89*(1), 54-68.

Satake, K. (2004). Detection of Kuril subduction-zone earthquakes from remote historic records in Honshu, Japan, between 1656 and 1867. *Annals of Geophysics, 47*(2-3).

Schwartz, S. Y., & DeShon, H. R. (2007). Distinct up-dip limits to geodetic locking and microseismicity at the northern Costa Rica seismogenic zone: Evidence for two mechanical transitions. The Seismogenic Zone of Subduction Thrust Faults, 576-599.

Seno, T., & Yamanaka, Y. (1996). Double Seismic Zones, Compressional Deep Trench-Outer Rise Events, and Superplumes. *Subduction Top to Bottom*, 347-355.

Stein, S., & Wysession, M. (2009). An introduction to Seismology, Earthquakes, and Earth Structure. Malden, MA: John Wiley & Sons.

Tectonic Summary: Seismotectonics of the Kuril-Kamchatka Arc. *M6.4 - 172km S of Ust'-Kamchatsk Staryy, Russia*. USGS, n.d. Retrieved on February 15, 2014 from http://comcat.cr.usgs.gov/earthquakes/eventpage/usb000kw1x#summary.

Tichelaar, B. W., & Ruff, L. J. (1993). Depth of seismic coupling along subduction zones. *Journal of Geophysical Research: Solid Earth (1978–2012),98*(B2), 2017-2037.

Wessel, P., Smith, W. H., Scharroo, R., Luis, J., & Wobbe, F. (2013). Generic mapping tools: Improved version released. *Eos, Transactions American Geophysical Union*, *94*(45), 409-410.

APPENDIX

SUPPLEMENTARY FIGURES

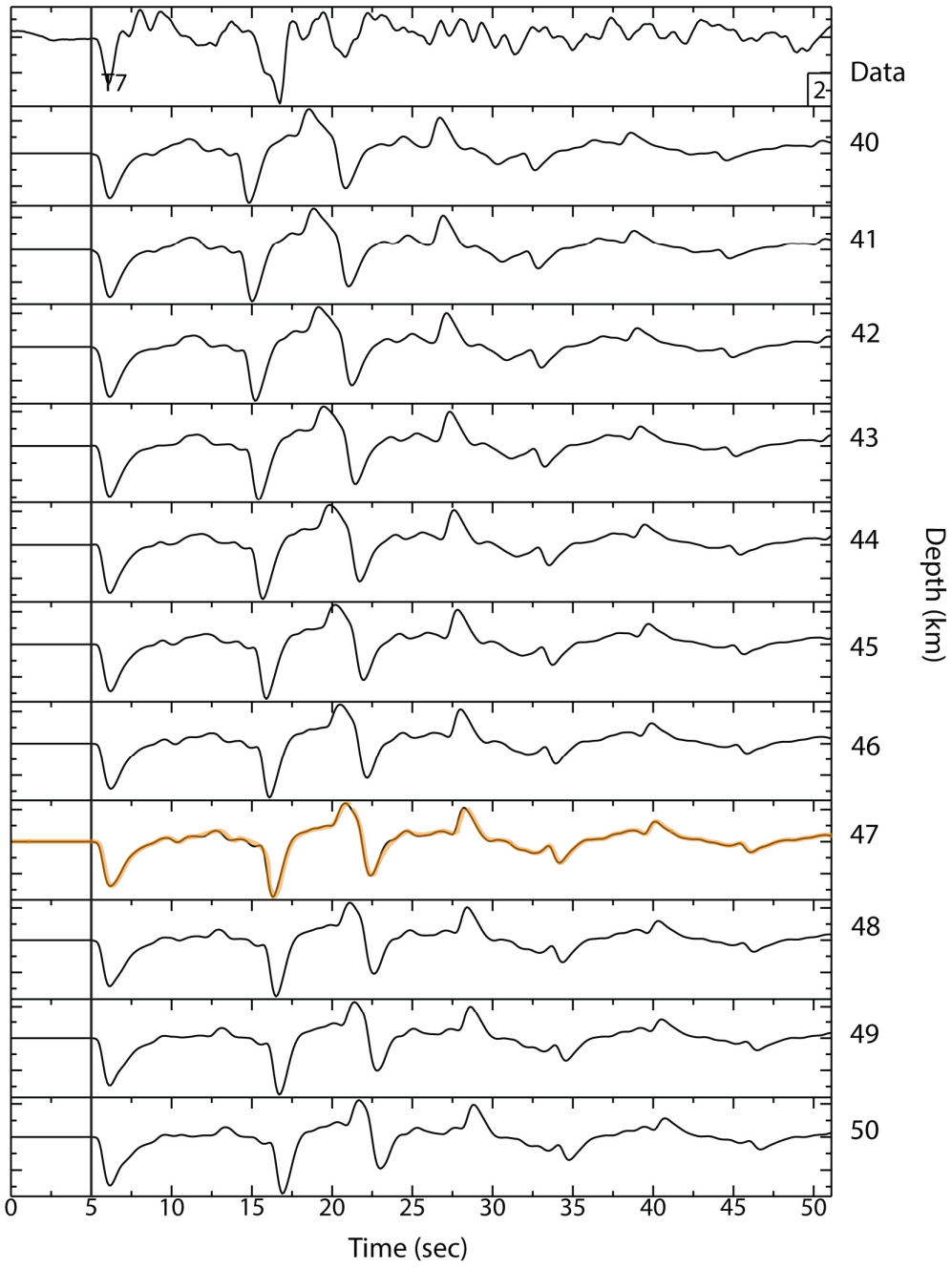

Figure A 1. Synthetics for compressional event on 9/10/90. Station WUS located at 295° azimuth and 55° distance from the event.

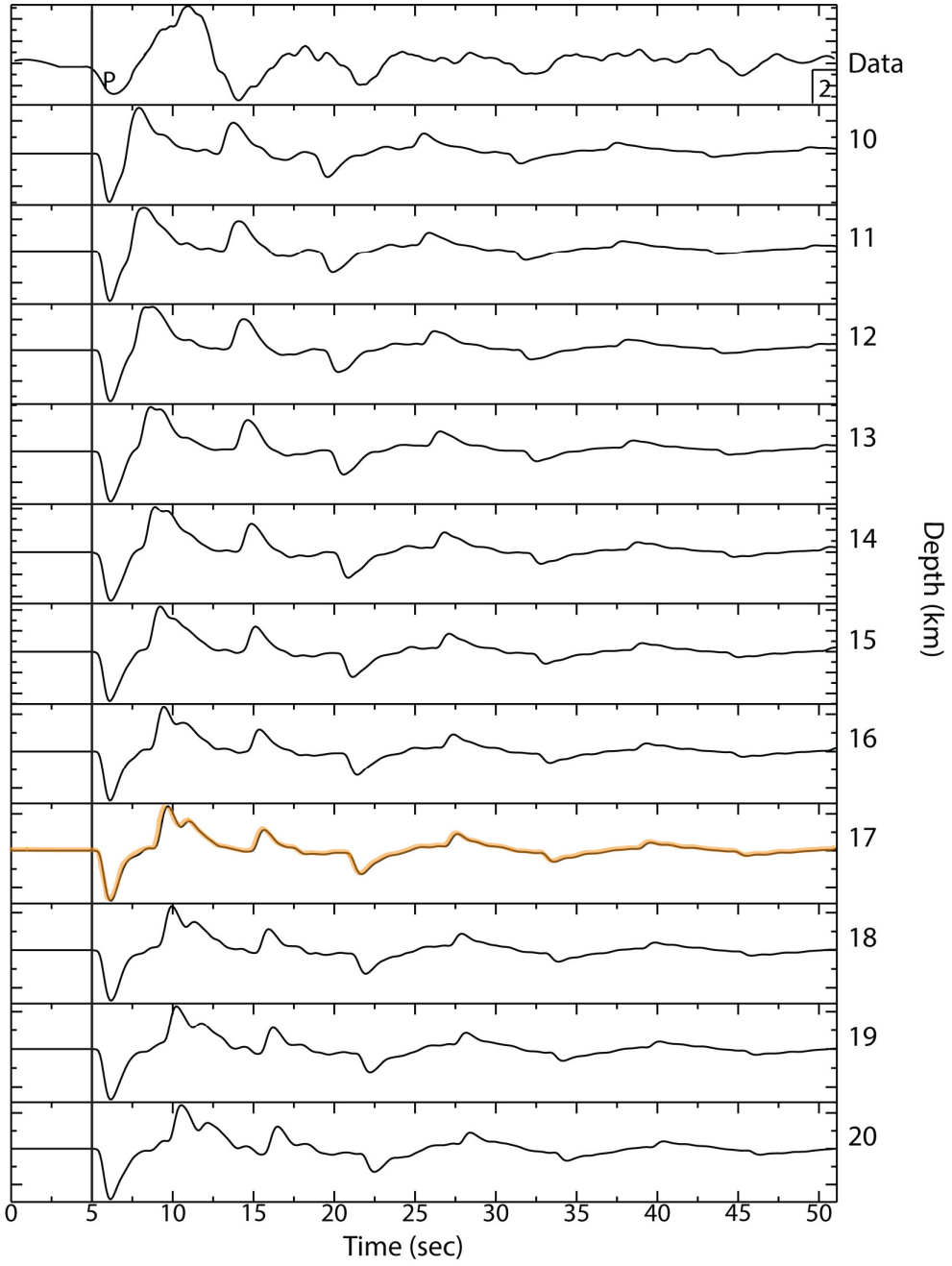

Figure A 2. Synthetics for tensional event on 9/5/1994. Station ANTO located at 320° azimuth and 80° distance from the event. Synthetics match closest at 17km.

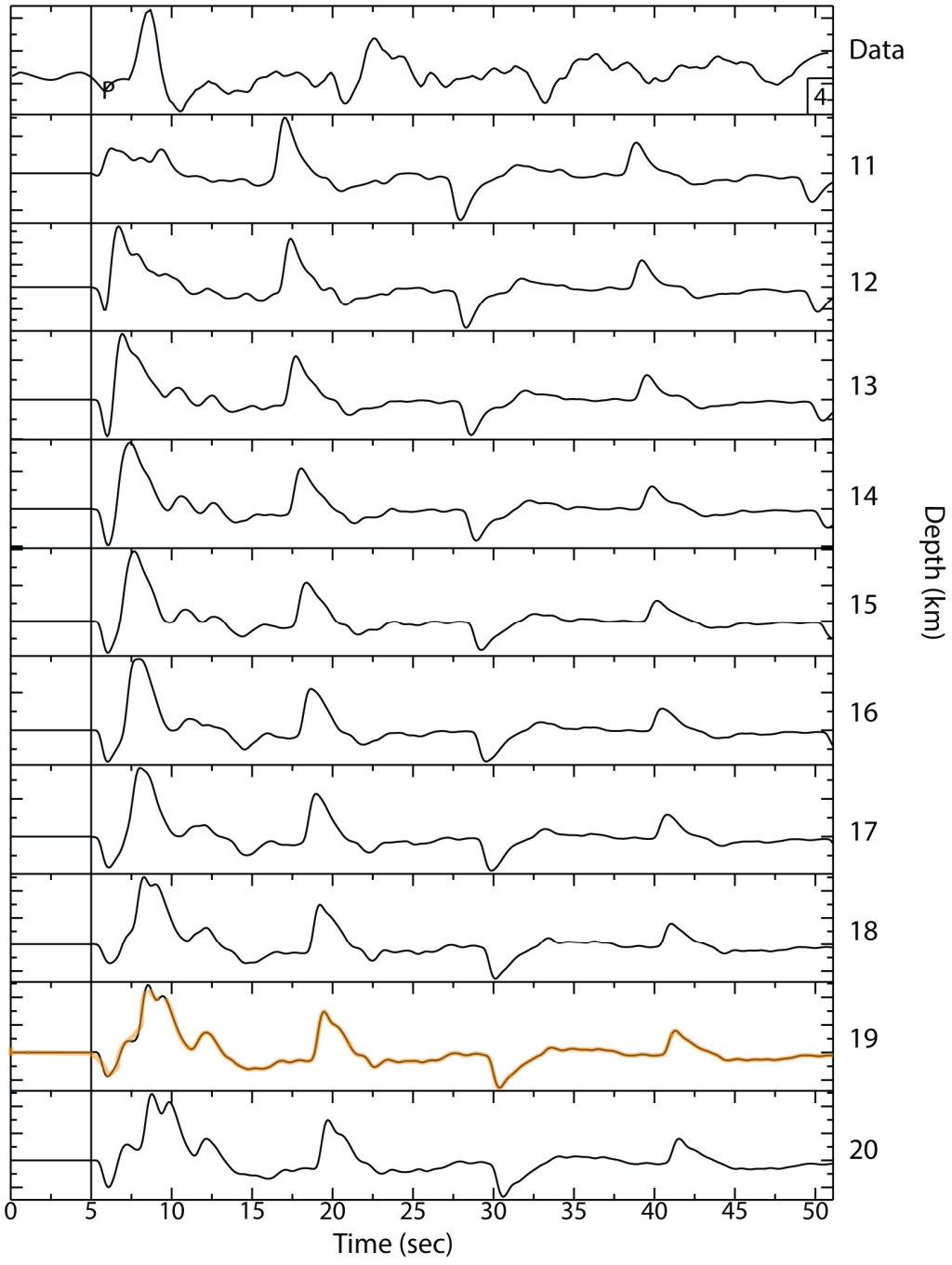

Figure A 3. Synthetics for a tensional event on 6/19/1995. Station ZRN located at 310° azimuth and 50° distance from event.

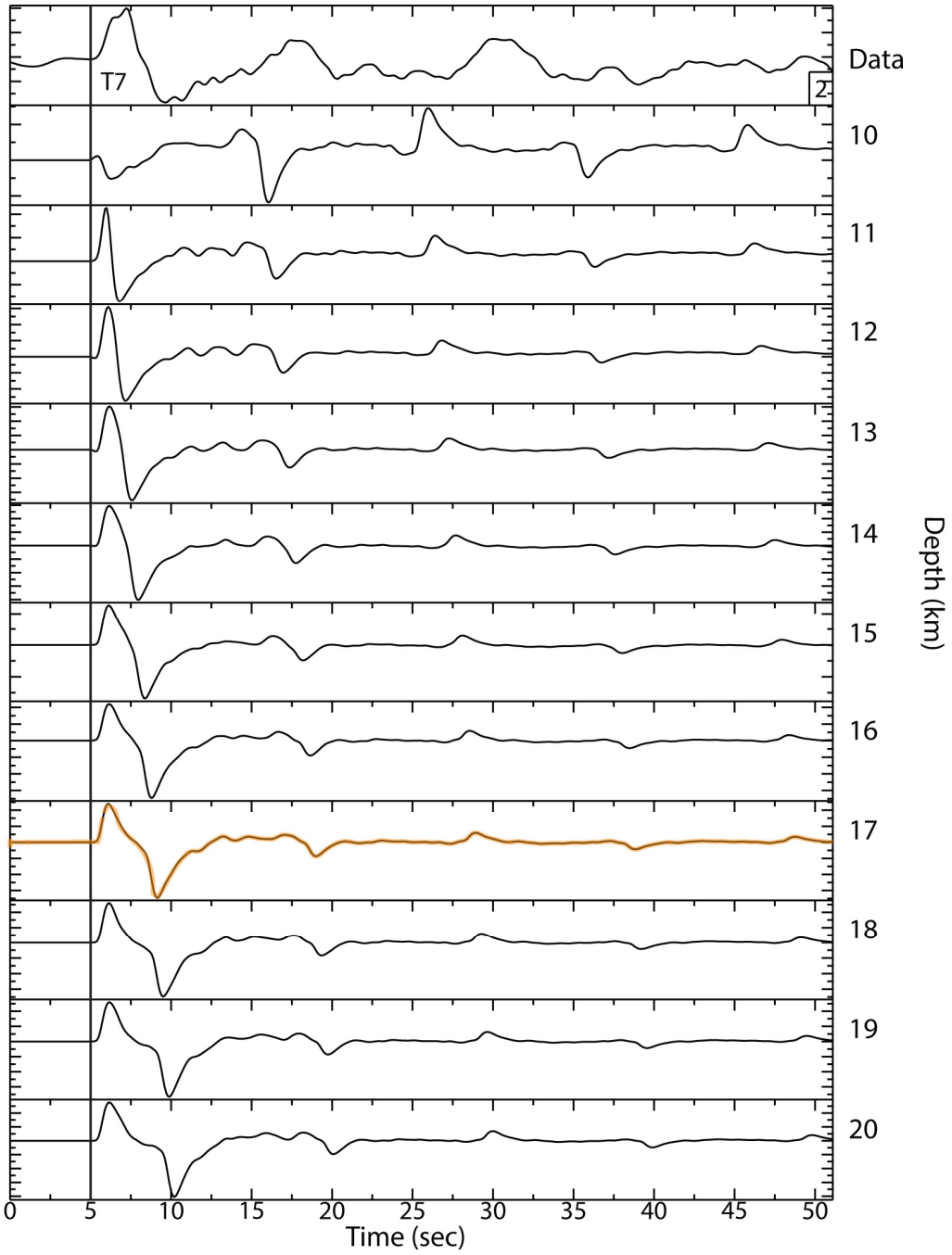

Figure A 4. Synthetics for a compressional event on 12/4/1995. Station WMQ located at 290° azimuth and 45° distance from event.

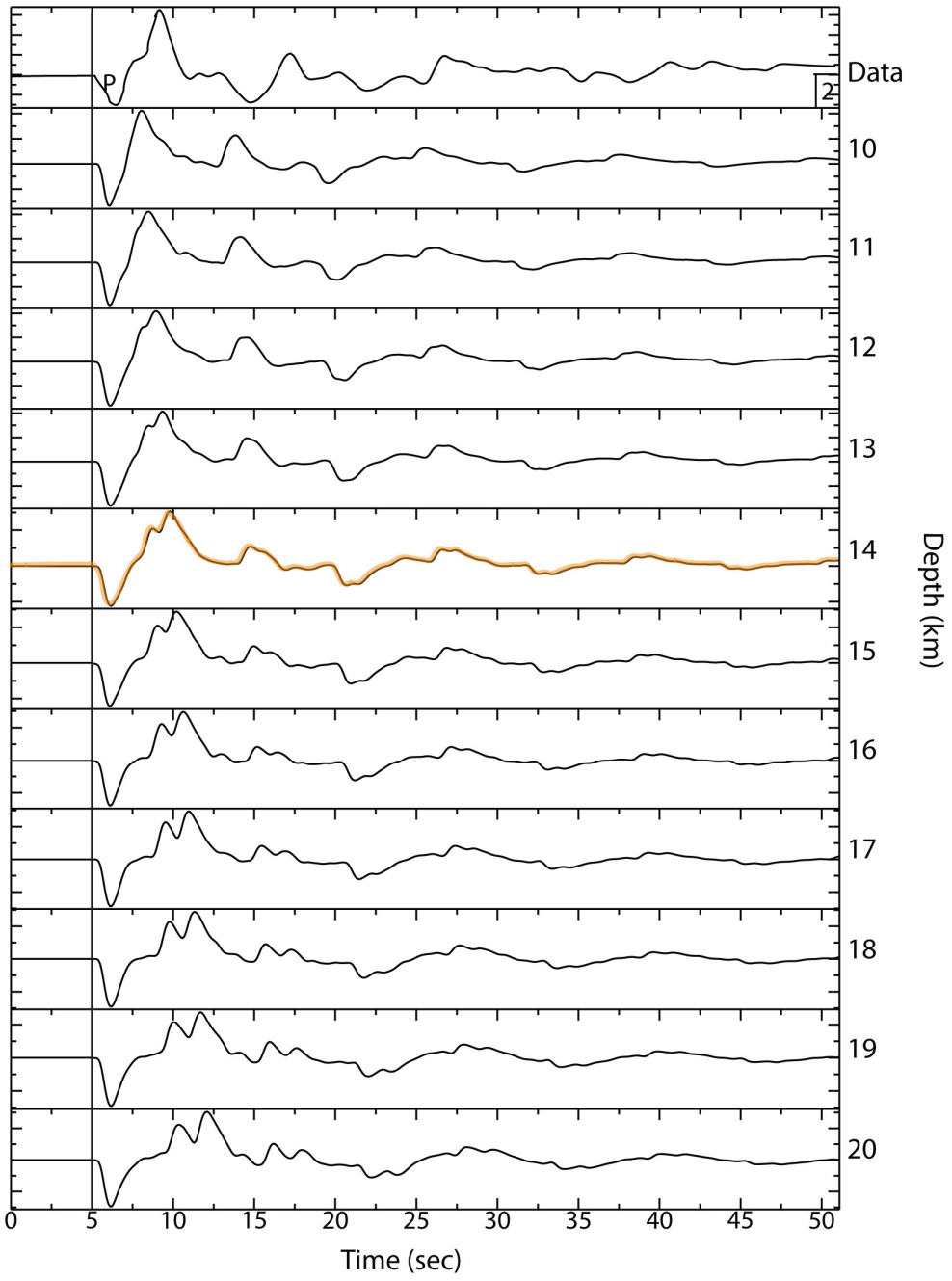

Figure A 5. Synthetics for tensional event on 9/13/2004. Station BRVK located 310° azimuth and 50° distance from event. Synthetics match closest at 14km.

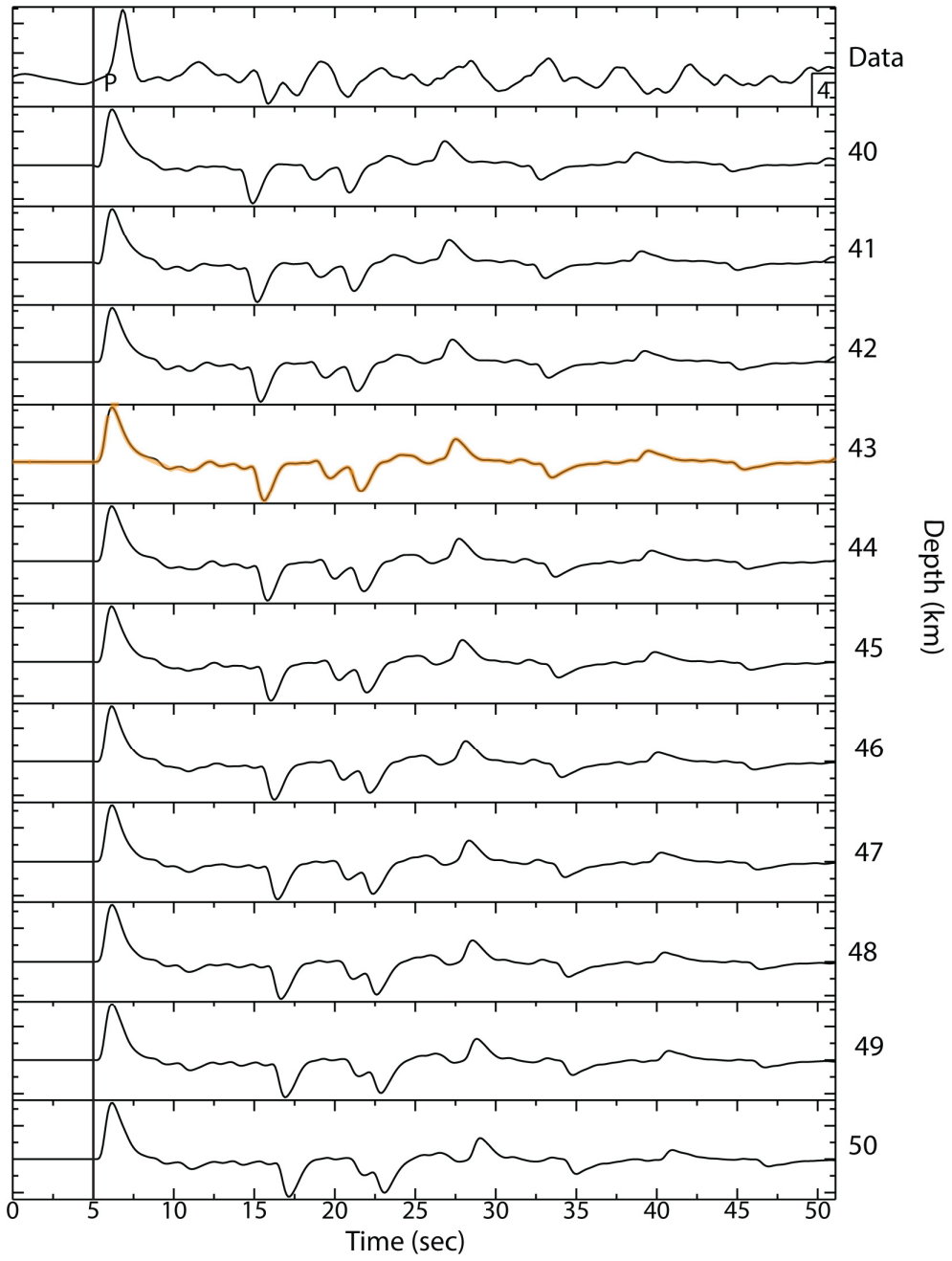

Figure A 6. Synthetics for compressional event on 8/10/2005. Station BOZ located at 55° azimuth and 60° distance from event. Synthetic matches best at depth of 43km.

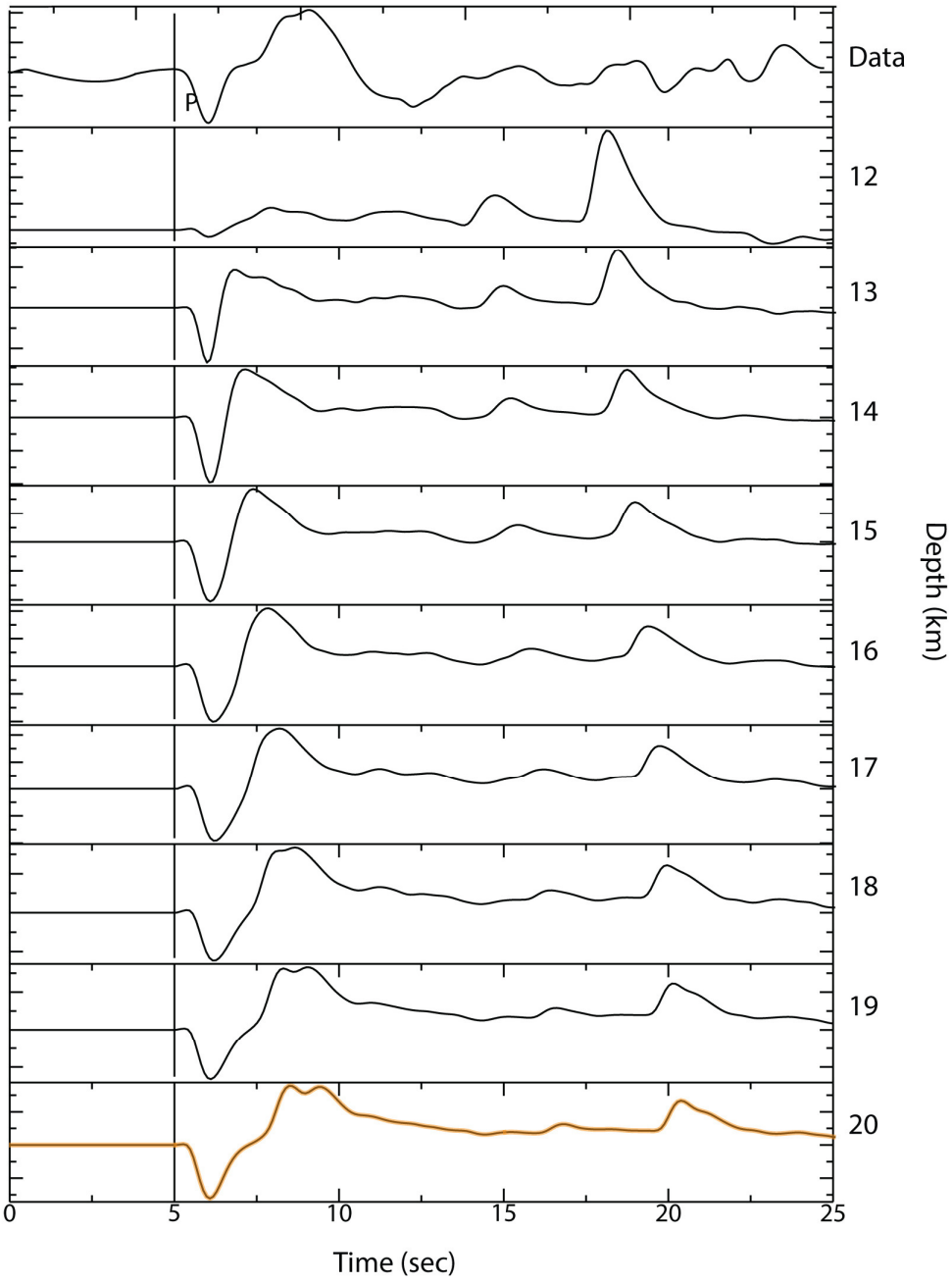

Figure A 7. Synthetics for tensional event on 11/19/2006. Station CHTO located at 260° azimuth and 55° distance from event. Synthetics match closest at 20km.

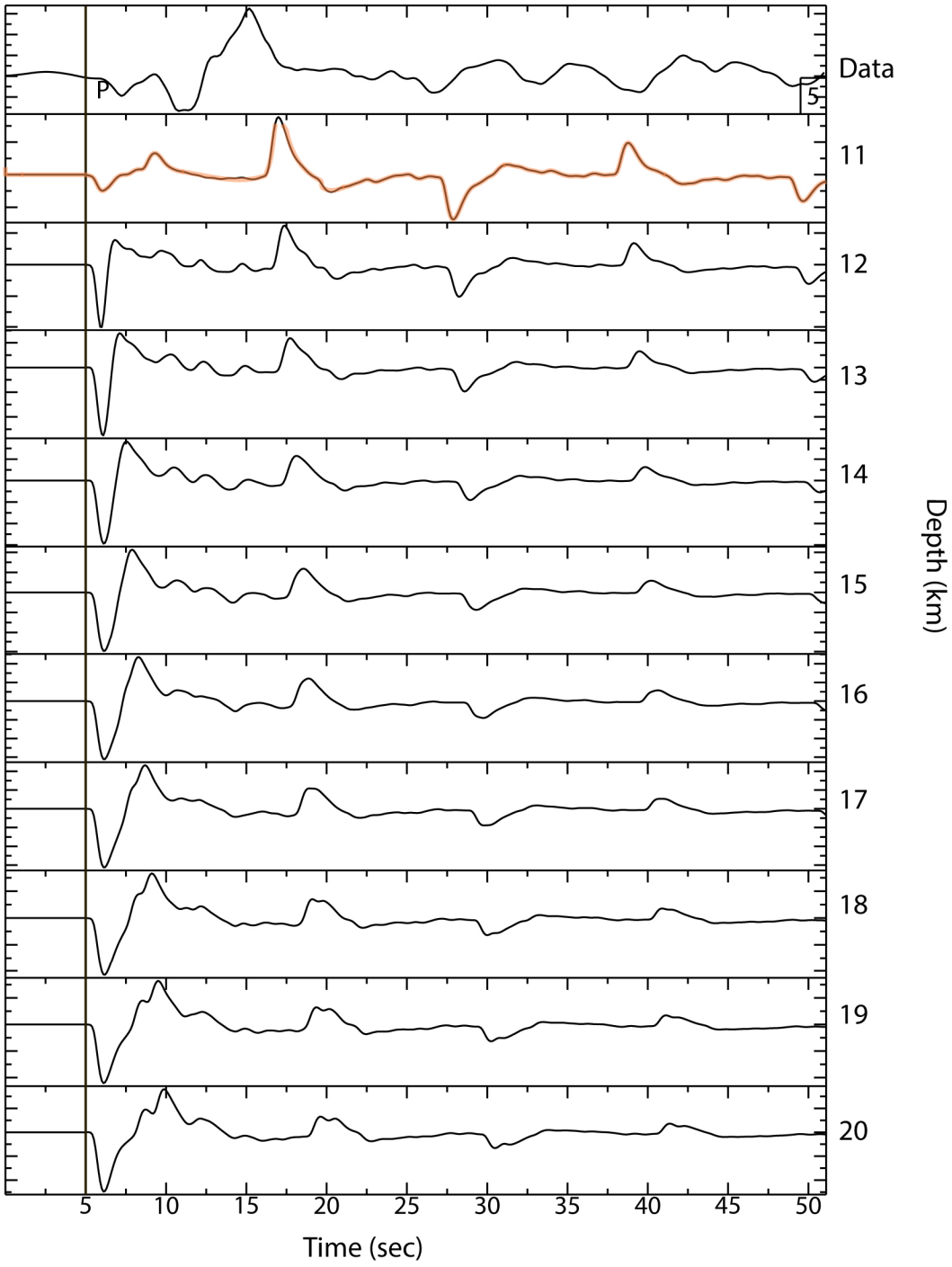

Figure A 8. Synthetics for a tensional event on 12/7/2006. Station BPAW located at 40° azimuth and 35° distance from the event. Synthetics match closest at 11km.

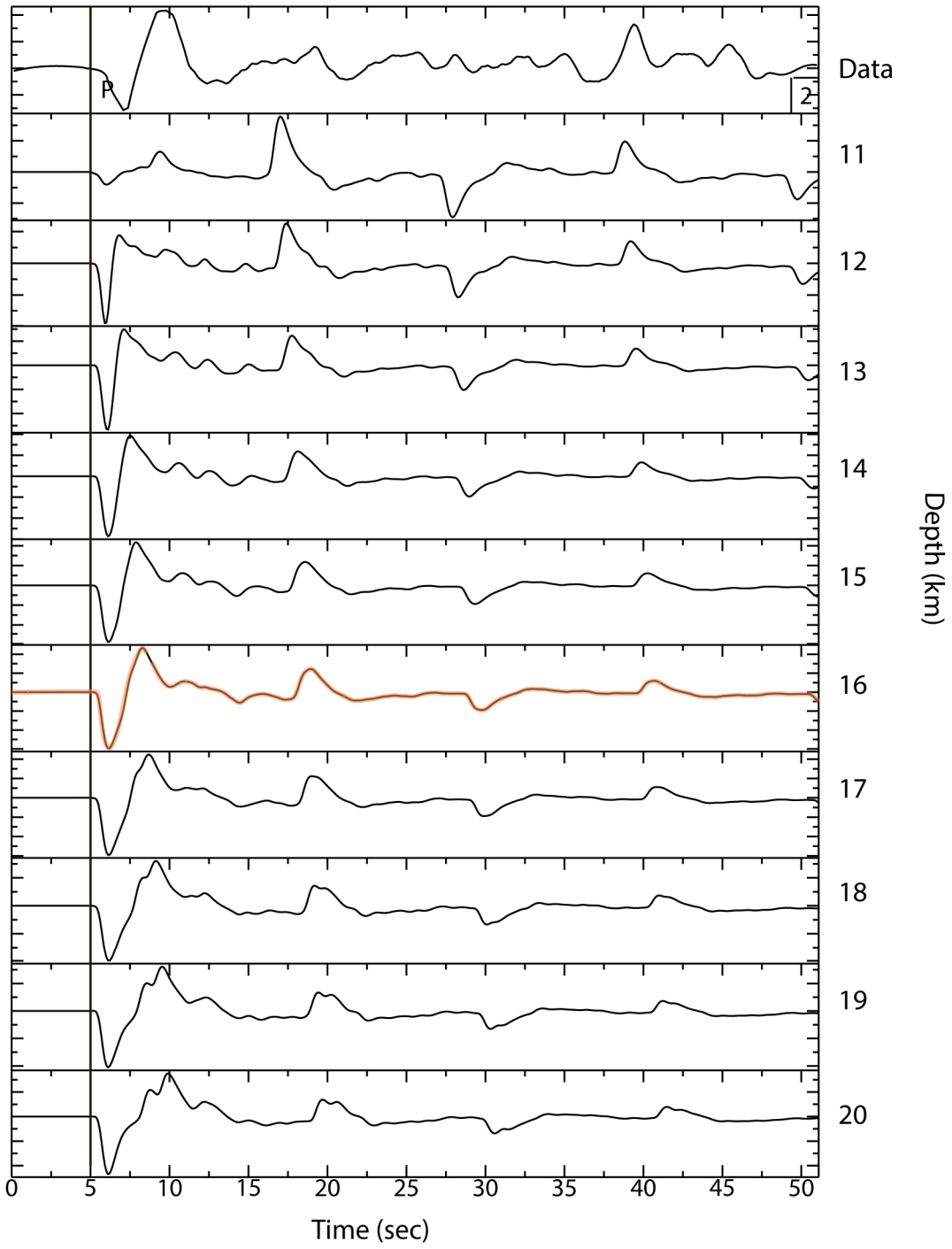

Figure A 9. Synthetics for a tensional event on 1/17/2009. Station KMI located at 260° azimuth and 45° distance from the event. Synthetics match closest at 11km depth.